

Gallium Nitride as an Electromechanical Material

Mina Rais-Zadeh, *Senior Member, IEEE*, Vikrant Jayant Gokhale, *Student Member, IEEE*,
Azadeh Ansari, *Student Member, IEEE*, Marc Faucher, Didier Théron, *Member, IEEE*,
Yvon Cordier, and Lionel Buchailot, *Member, IEEE*

Abstract—Gallium nitride (GaN) is a wide bandgap semiconductor material and is the most popular material after silicon in the semiconductor industry. The prime movers behind this trend are LEDs, microwave, and more recently, power electronics. New areas of research also include spintronics and nanoribbon transistors, which leverage some of the unique properties of GaN. GaN has electron mobility comparable with silicon, but with a bandgap that is three times larger, making it an excellent candidate for high-power applications and high-temperature operation. The ability to form thin-AlGaIn/GaN heterostructures, which exhibit the 2-D electron gas phenomenon leads to high-electron mobility transistors, which exhibit high Johnson's figure of merit. Another interesting direction for GaN research, which is largely unexplored, is GaN-based micromechanical devices or GaN microelectromechanical systems (MEMS). To fully unlock the potential of GaN and realize new advanced all-GaN integrated circuits, it is essential to cointegrate passive devices (such as resonators and filters), sensors (such as temperature and gas sensors), and other more than Moore functional devices with GaN active electronics. Therefore, there is a growing interest in the use of GaN as a mechanical material. This paper reviews the electromechanical, thermal, acoustic, and piezoelectric properties of GaN, and describes the working principle of some of the reported high-performance GaN-based microelectromechanical components. It also provides an outlook for possible research directions in GaN MEMS. [2014-0147]

Index Terms—III-V, HEMT, microelectromechanical systems, micromachining, piezoelectric materials, resonators, wide bandgap.

I. INTRODUCTION

OVER THE recent few years, GaN has become one of the most popular semiconductor materials [1]–[3]. As with any other growing industry, fundamental breakthroughs in material science and device technologies have been aided by rapid improvements in the fabrication and processing

Manuscript received May 8, 2014; revised July 11, 2014; accepted August 22, 2014. This work was supported in part by the U.S. National Science Foundation under Award 1002036 and Award 1055308; in part by the U.S. Army Research Laboratory, Adelphi, MD, USA, through the Micro Autonomous Systems and Technology Collaborative Technology Alliance under Contract W911NF; and in part by the French National Research Agency under Contract ANR-08-NANO-023. Subject Editor G. Piazza.

M. Rais-Zadeh, V. J. Gokhale, and A. Ansari are with the University of Michigan, Ann Arbor, MI 48109 USA (e-mail: minar@umich.edu; vikrantg@umich.edu; azadans@umich.edu).

M. Faucher, D. Theron, and L. Buchailot are with the Institut d'Electronique de Microelectronique et de Nanotechnologie, Villeneuve d'Ascq 59652, France (e-mail: marc.faucher@isen.iemn.univ-lille1.fr; didier.theron@iemn.univ-lille1.fr; lionel.buchailot@iemn.univ-lille1.fr).

Y. Cordier is with the Centre de Recherche sur l'Hétéro-Epitaxie et ses Applications, Valbonne 06560, France (e-mail: yvon.Cordier@crhea.cnrs.fr).

Color versions of one or more of the figures in this paper are available online at <http://ieeexplore.ieee.org>.

Digital Object Identifier 10.1109/JMEMS.2014.2352617

TABLE I

PROPERTIES OF A SELECTION OF ELECTROMECHANICAL MATERIALS

Material	Elastic Modulus c_{33} (GPa)	Acoustic Velocity (m/s)	Piezoelectric Coefficient e_{33} (Cm ⁻²)	$f \times Q^+$ (Hz)	k_{eff}^2 (%)	Ref
Si	165	8415	N/A	2.5×10^{13}	N/A	[4]
SiC	605	13100	+0.2	3.5×10^{14}	0.08	[4-7]
GaAs	118	2470	-0.16	-- [†]	0.04	[8, 9]
AlN	390	11000	+1.55	10^{13}	5.6	[4, 10]
Sc doped AlN	244	8509	+3.9	3×10^{11}	15.5	[11, 12]
LiNbO ₃ (X-cut) [‡]	60	3900	+3.65	7.7×10^{11} (measured)	16	[13, 14]
GaN	398	8044	+0.65	2.5×10^{13} (theory) 5×10^{12} (measured)	2	[4, 15-18]

* For anharmonic phonon scattering in Akhieser regime

[†] Data not available

[‡] LiNbO₃ data are for shear mode, not longitudinal mode

techniques [1], [2] with consistent improvements in wafer size, material quality, diversification of epitaxial substrate material, and ease of market access. While the current cost of GaN substrates is high, based on the economics of scale, high-volume production of GaN wafers is expected to reduce the wafer cost to the same level as GaAs substrates [1]. In addition, epitaxial growth of high-quality GaN on low-cost substrates, such as silicon (Si), is becoming more mature. This would make GaN one of the cheapest semiconductors, second only to Si.

The growth of GaN semiconductor industry has been fueled primarily by those segments devoted to optoelectronics, driving material improvement, followed by high-power electronics and radio-frequency (RF) electronics, which take advantage of the wide bandgap and high breakdown capabilities of this material. While a significant amount of scientific research has been devoted to the applications mentioned above, little attention has been given to the use of GaN for nano and microelectromechanical systems (N/MEMS). Unlike Si, GaN is a piezoelectric semiconductor and one can envision using the piezoelectric properties of GaN alone to manufacture multitude of devices for diverse applications. Besides being a piezoelectric, GaN offers several other advantages as an electromechanical material.

A selection of some of the pertinent material figures of merit (FOM) of GaN is compared with a selection of other commonly used electromechanical materials in Table I. It can be seen that GaN is one of the most

versatile materials available for use in electromechanical systems.

A large amount of research has gone into characterizing the growth, processing, electrical and optical properties of GaN. However, broader understanding of the material is necessary in order to explore more applications that can be enabled by affordable high-quality GaN. The purpose of this work is to provide the most recent data on the electromechanical properties of GaN grown epitaxially on Si substrates, review its current use in MEMS applications with a special focus on RF MEMS and GaN resonant microdevices, and provide possible directions for GaN NEMS/MEMS research.

II. ELECTROMECHANICAL PROPERTIES OF GaN

A. Crystallinity of GaN on Si

A wide range of techniques have been used to grow thin-film GaN on a substrate, such as metal organic vapor phase epitaxy (MOVPE) and molecular beam epitaxy (MBE). A variety of substrates such as Si, silicon carbide (SiC), and sapphire have been used for these studies [2]. Most of the films grown have wurtzite crystalline structure and have n-type conductivity [2], although Zinc blende GaN growth has also been reported. Intentional p-type doping of GaN is also possible [19]. In this paper, we focus on properties of GaN grown on Si. GaN-on-Si substrates are attractive candidates for GaN MEMS and GaN movable mechanical components with Si selectively removed underneath GaN structures. GaN-on-Si is also an attractive substrate for implementing GaN devices integrated with Si-based large scale integrated circuits, although the highest quality GaN films have been obtained on Si (111) or Si (110) and not on Si (100).

GaN in its wurtzite form has a crystal structure with lattice parameters of $a = 3.189\text{\AA}$ and $c = 5.185\text{\AA}$. A figure of merit that is commonly used to characterize the intrinsic crystalline quality of an epitaxially grown thin film is the Full Width at Half Maximum (FWHM) acquired using X-Ray Diffraction (XRD) analysis. A narrow FWHM denotes high long-range crystalline order and good internal alignment of the crystal (Fig. 1). However, special care has to be taken concerning the symmetric (000 l) XRD reflection line width, which in the case of thick films is mostly sensitive to the so-called (low-density) screw-type threading dislocations. XRD reflection lines measured for oblique crystal planes, such as (10-12) or (30-32), are much more relevant because they are sensitive to almost all the threading defects. However, these are sometimes not reported.

To achieve good FWHM values for GaN-on-Si, it is often necessary to grow a thin layer of AlN or a graded AlN/AlGaIn buffer layer to avoid chemical reactions between gallium and silicon and to accommodate the lattice mismatch between the substrate and the epitaxial GaN. Table II lists reported (0002) XRD FWHM values of GaN grown on the most commonly used substrates. It should be noted that the recent results for GaN-on-Si [20] demonstrated by Pinos *et al.* in 2014 exhibit FWHM values comparable to high-quality GaN films grown on sapphire [21], [22]. Recent results

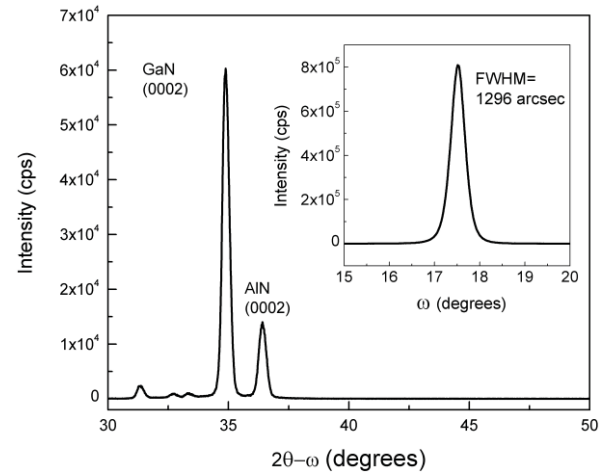


Fig. 1. A representative result showing XRD spectroscopy on a GaN thin film grown on a Si (111) substrate using metal-organic chemical vapor deposition (MOCVD). Inset: Rocking curve of the (0002) GaN plane exhibits a very clear peak and a FWHM of 1296 arcsec. Films were measured using a Rigaku Ultima IV XRD system.

TABLE II
CRYSTALLINE QUALITY OF THIN FILM GaN

Substrate	Growth Technique	FWHM (arcsec)	Year	Ref.
c-Sapphire	MOVPE	300	2003	[21]
c-Sapphire	MOVPE	250	2013	[22]
(111) SOI	MOVPE	1368	2005	[23]
(111) SOI	MOVPE	1926	2013	UM
(111) Si	MOVPE	1396	2011	[17]
(111) Si	MOVPE	1296	2014	UM
(111) Si	MOVPE	700	1993	[24]
(111) Si	MBE	317	2010	[16]
(111) Si	MOVPE	343	2014	[20]

measured at the University of Michigan (UM) are acquired using a Rigaku Ultima IV X-ray diffractometer, on bare, unprocessed GaN films.

B. In-Situ Stress Measurements During Growth

In-situ wafer curvature measurements are helpful to understand the evolution of the stress profile within the grown materials. Here, an MBE reactor is used to grow GaN-on-Si on AlN nucleation layers with an initial compressive strain related to the in-plane lattice parameter mismatch of 2.5% between the two materials. A large part of the mismatch is rapidly relaxed via the introduction or the bending of dislocations. However, depending on the epitaxial layer sequence grown before the final GaN layer, the remaining part of the stress can vary significantly within the layer. In these structures AlN is grown at 920 °C and GaN at 800 °C. Fig. 2 illustrates the variation in the substrate curvature while growing a 1 μm thick GaN film on a 0.2 μm AlN nucleation layer compared to a 1.7 μm GaN film on AlN/GaN/AlN (80 nm/0.25 μm /42 nm) stress mitigating stack.

In the absence of inter-layers, the compressive stress in GaN grown on AlN is rapidly relaxed and the negative curvature

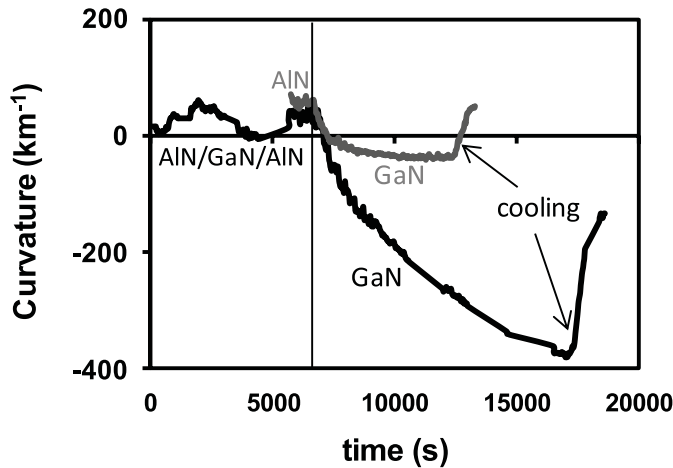


Fig. 2. Substrate curvature for GaN films grown by MBE on AlN (gray) and on AlN/GaN/AlN stress mitigating (black) layers. The addition of the stress mitigating layers enables the growth of thick GaN structures on a Si substrate.

(convex bowing) saturates at a rather low level before it reaches positive values (concave bowing) upon cooling down at the end of the growth (here from 800 °C to room temperature (RT)). Such a behavior upon cooling is caused by the mismatch between the thermal expansion coefficient (TEC) of GaN and Si. On the contrary, GaN grown on stress mitigating layers induces a noticeable convex substrate bowing even after growth of more than 1.7 μm thick GaN [25]. Moreover, the non-linear evolution of the curvature accounts for the presence of a stress gradient varying from compressive in the vicinity of the interface with AlN to almost relaxed towards the surface. Such a structure is able to maintain a convex substrate bowing upon cooling down in spite of its larger thickness. This way, thick structures can be grown crack-free with a better crystal quality, but with a risk of buckling while releasing membranes or clamped beams. One important point is that the stress responsible for the substrate bowing at the growth temperature is still present at room temperature, but shifted by the additional stress (~ 1 GPa) due to the TEC mismatch between GaN and Si. Then, as compared to growth temperature, the stress profile shall be almost unchanged at room temperature after the release from the substrate. Thus, the in-situ curvature measurement is helpful to understand the behavior of released beams or membranes. As shown in Fig. 3, low-temperature photoluminescence [25] performed on GaN layers of various thicknesses with and without stress mitigating layers confirms the presence of stress gradients. In simple structures, a tensile stress develops from almost zero up to 1 GPa, confirming the rapid stress relaxation in GaN at the growth temperature. In the presence of stress mitigating stacks, the stress ranges from about -2 GPa (compressive) in the bottom part of the GaN film up to less than $+0.3$ GPa (tensile) in the upper part. When releasing the structures from the substrate, the data plotted in Fig. 3 shall be shifted by -1 GPa. It is worth to mention that the efficiency of the inter-layers for stress mitigation depends on the crystal quality of the nucleation process, which itself affects the required thickness of each stress-mitigation layer: for instance, progress in Si surface preparation led us to reduce the AlN inter-layer

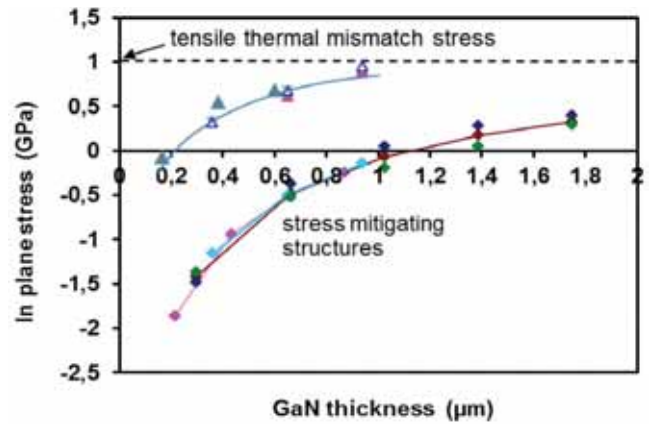


Fig. 3. In-plane stress acquired using low-temperature photoluminescence measurements for GaN layers with various thicknesses, grown on multiple samples. A marked difference is seen due to the presence (diamonds) or absence (triangles) of stress mitigating layers. Each color represents data for one sample. The lines are guides for the eyes.

thickness from 0.25 μm in [25] down to 75 nm in some cases. The 0.25 μm GaN can also be replaced by a 0.25 μm $\text{Al}_{0.15}\text{Ga}_{0.85}\text{N}$ inter-layer for a better electrical isolation [26]. Even when other thicknesses are used, the principle of inter-layers has shown its efficiency for growing thick GaN films on Si by MOVPE (Table III) [27].

At present, good crystal quality samples have been developed on structures with buffer layers not optimized for MEMS applications while efforts have to be made in the future to enhance the crystal quality of simple thin structures (without stress mitigating stacks) that are more promising from a mechanical point of view. As the risk of layer cracking before the release from the substrate is higher in the absence of stress mitigating stacks, it is crucial to grow optimized films carefully to get GaN films with reasonable total stress before and upon the release from the substrate.

C. Mechanical Properties of GaN

The mass density of GaN has been quoted in the literature as 6095 kg/m^3 [28], [29] or 6150 kg/m^3 [2]. Due to its hexagonal nature, the elastic properties of wurtzite GaN are symmetric along the in-plane vectors. The elastic moduli of w-GaN have been calculated by Wright using ab-initio density field calculations [30] and verified using Brillouin scattering by Yamaguchi *et al.* [31] and Polian *et al.* [28]. The full stiffness matrix for GaN is given by C_{ij} , as shown at the bottom of the next page.

The elastic compliance and constants for the binary compounds as well as the rule to obtain the values for alloys are summarized by Ambacher *et al.* [2]. Knoop hardness of GaN was reported to be 14.21 GPa [2] and agrees well with experimental data obtained for GaN-on-Si samples in this work (Table III). The majority of these films are grown with inter-layers to avoid cracks.

The microhardness of single crystal GaN thin films is reported to be 10.2–19 GPa [2], [37]. In order to verify the previously reported values, nanoindentation experiments were carried out recently at both University of Michigan

TABLE III
MECHANICAL PROPERTIES OF GaN (IL STANDS FOR INTER-LAYERS)

Substrate	Fabrication Technique / GaN thickness	Hardness (GPa)	Young's modulus (GPa)	Indenter tip	Ref.
Bulk	-	12 ± 2	287	Vickers	[32]
Bulk	-	18-20	295 ± 3	Berkovich	[33]
c-Sapphire	MOVPE/1.3-2.4 μm	53.6	290	Berkovich	[34]
c-Sapphire	MOVPE/1.8-4 μm	15.5 ± 0.9	210 ± 23	Spherical	[35]
c-Sapphire	MOVPE/ 2 μm	19 ± 1	286 ± 25	Berkovich	[36]
ILs/(111) Si	MBE/ 2 μm	22.7 ± 3	266 ± 43	Berkovich	UM
c-Sapphire	MOVPE/ 1 μm	25.5 ± 0.6	405 ± 7	Berkovich	UM
ILs/SOI	MOVPE/ 1.5 μm	23 ± 2.3	288 ± 21	Berkovich	UM
ILs/(111) Si	MOVPE/ 3 μm	22.8 ± 0.9	311 ± 24.6	Berkovich	IEMN
c-Sapphire	MBE/ 4 μm	24.6 ± 1.2	331 ± 25.3	Berkovich	IEMN
ILs/(111) Si	MBE/ 5 μm	22.4 ± 2.4	303 ± 27	Berkovich	IEMN
(111) Si	MBE/ 1 μm	22.3 ± 1.6	261 ± 19.2	Berkovich	IEMN
ILs/(111) Si	MBE/ 1 μm	23.4 ± 1.3	274 ± 15.4	Berkovich	IEMN

and at IEMN. These previously unpublished results largely support prior data. Here, nanoindentation experiments leading to the mechanical properties of GaN films have been obtained by means of a MTS NanoXP® nanoindenter (Agilent Technologies Inc., Oak Ridge, TN, USA) at IEMN using a Berkovich tip. The equipment is installed in a clean-room where temperature and humidity are monitored and maintained constant. A NanoInstruments Nanoindenter II with a Berkovich tip was used at UM. Both sets of nanoindentation measurements were performed on bare samples of the specified GaN film using the continuous stiffness measurement (CSM) method, where a small oscillation is superimposed to the primary loading signal [38]. Nanoindentation tests carried out in the course of this work indicate that the hardness for different types of substrates and fabrication methods consistently lies in the range of 20-26 GPa (Fig. 4). GaN Young's moduli reported in Table III are higher when the material is directly grown on bulk c-Sapphire or when the layers are thick enough on (111) Si substrate. It is significantly lower when the thickness of GaN grown on Si is inferior to 3 μm (Fig. 5), indicating probable influence of the crystal quality on the Young's modulus.

D. Piezoelectric Properties of GaN

The use of GaN as an electromechanical material is predicated on its piezoelectric properties. Piezoelectric actuation can be used for both static as well as dynamic actuation/sensing, with frequencies as high as tens of GHz. As a piezoelectrically actuated vibrating or resonant system,

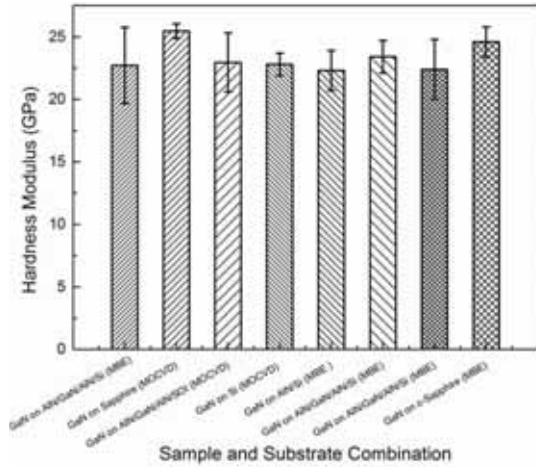


Fig. 4. Hardness for eight different GaN films used in this work. The data are measured using a Berkovich tip nanoindenter. The values represent an average of at least eight indents on each sample.

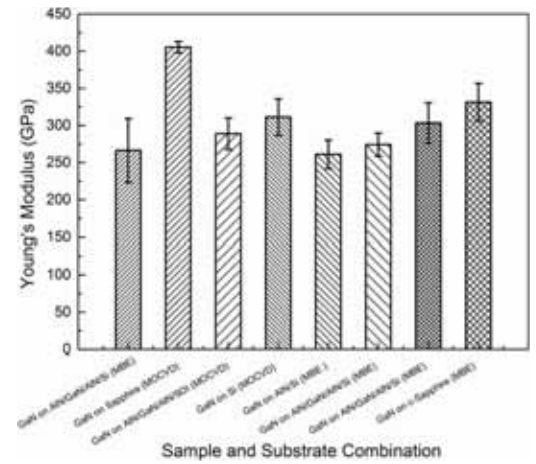


Fig. 5. Young's modulus for eight different GaN films used in this work. The data are measured using a Berkovich tip nanoindenter. The values represent an average of at least eight indents on each sample.

GaN has the advantage of high coupling efficiency compared to similar devices using capacitive, thermal, or magnetic actuation. A large number of devices discussed in this review are based on the piezoelectric transduction principle. The piezoelectric coefficients of wurtzite GaN have been calculated by Bykhovski *et al.* [39] to be

$$e_{ij} = \begin{pmatrix} 0 & 0 & 0 & 0 & -0.3 & 0 \\ 0 & 0 & 0 & -0.3 & 0 & 0 \\ -0.33 & -0.33 & +0.65 & 0 & 0 & 0 \end{pmatrix} Cm^{-2}$$

$$C_{ij} = \begin{pmatrix} 390 \pm 25 & 145 \pm 20 & 106 \pm 20 & 0 & 0 & 0 \\ 145 \pm 20 & 390 \pm 15 & 106 \pm 20 & 0 & 0 & 0 \\ 106 \pm 20 & 106 \pm 20 & 398 \pm 20 & 0 & 0 & 0 \\ 0 & 0 & 0 & 105 \pm 10 & 0 & 0 \\ 0 & 0 & 0 & 0 & 105 \pm 10 & 0 \\ 0 & 0 & 0 & 0 & 0 & 122.5 \pm 20 \end{pmatrix} GPa$$

These and very similar values [40] are popularly used by many subsequent researchers. Bernardini *et al.* [41] and Shur *et al.* [42] calculate different values of 0.73 Cm^{-2} and -0.49 Cm^{-2} for e_{33} and e_{31} , respectively. Cimalla *et al.* [2] reported similar vales in a review of a number of theoretical and measured results (using interferometry and atomic force microscopy) for the piezoelectric constants of GaN and concluded that the film structure and quality highly influences the exact numbers.

E. Thermal Properties of GaN

As a material intended for high-power or high-temperature electronics and capable of operating in harsh environments, it is useful to know the thermal properties of GaN. The thermal conductivity of GaN is highly dependent on the film quality, the concentration and type of impurities and defects present, and the temperature. Experimental results for thermal conductivity of GaN indicate that the room temperature values for thermal conductivity are within the range of 100 W/m-K to 250 W/m-K [43]–[45]. The thermal conductivity shows an inverse relation with the doping and impurity concentration [46], [47]. The decrease was attributed mostly to the increased phonon relaxation on dopants. Measured values agree well with theoretical estimates [48]. The Debye temperature for wurtzite GaN has been calculated as 618 K to 641 K [31], [49]. The specific heat capacity of GaN is in the range of 300 J/kg-K to 500 J/kg-K at room temperature [6], [50]. GaN coefficient of thermal expansion (β) is on the order of $3 \times 10^{-6} \text{ K}^{-1}$ along the c-axis [6], [50], and in the range of $3.8 \times 10^{-6} \text{ K}^{-1}$ to $5.6 \times 10^{-6} \text{ K}^{-1}$ in-plane [6], [50]. GaN is also known to be a very strong pyroelectric material [42], [51] with an expected pyroelectric voltage coefficient ($P_v = 7 \times 10^5 \text{ V/m-K}$) greater than the proven high-temperature pyroelectric material lithium tantalite ($P_v = 5 \times 10^5 \text{ V/m-K}$) [42]. Experimental results have demonstrated values of P_v up to $1 \times 10^4 \text{ V/m-K}$ [51] and further investigation is necessary to utilize the full potential of GaN-based pyroelectric devices.

F. Electrical Properties of GaN

Extensive research has been recently conducted on compound semiconductor materials, motivated by their superior material properties as compared to Si. GaN, as the second most popular semiconductor, with a bandgap energy of $E_g = 3.4 \text{ eV}$ at room temperature, offers high breakdown electric field, high thermal conductivity, high peak velocity, and high saturation velocity. Further contributing to the outstanding material properties of GaN, is the ability to achieve two-dimensional electron gases (2DEG) with sheet carrier concentrations of more than 10^{13} cm^{-2} and high electron mobility of more than $2000 \text{ cm}^2/\text{V-s}$ at AlGaIn/GaN hetero-interface without intentional doping. The excellent electrical properties of AlGaIn/GaN high electron mobility transistors (HEMTs) make it a perfect candidate for high-frequency, high-temperature, and high-power operations. Particularly, AlGaIn/GaN hetero-structures, show clear advantages over other material systems such as GaAs, SiC, and Si

TABLE IV
ELECTRICAL PROPERTIES OF GaN

Properties	Si	GaAs	SiC	InP	GaN
μ (electron mobility) ($\text{cm}^2/\text{V-sec}$)	1400	10^3 *	800	5400	2000*
E_g (bandgap) (eV)	1.1	1.4	3.26	1.34	3.4
E_{br} (breakdown field) (MV/cm)	0.3	0.4	3.5	0.5	3.3
V_{sat} (Saturation velocity) ($\times 10^7 \text{ cm/s}$)	1.0	1.5	2	0.67**	2.5
n_c (density) ($\times 10^{17} \text{ cm}^{-2}$)	<1	~ 1 *	-	3*	15*
Johnson's FoM***	1.0	2.7	20	0.33	27.5
Baliga's FoM***	1.0	9.6	3.1	22.3	24.6
T_{max} ($^\circ\text{C}$)	300	300	600	300	700

* Measured values of the corresponding hetero-structure.

** Measured value at $E = 500 \text{ KV/cm}$.

*** Reported values are normalized to Si.

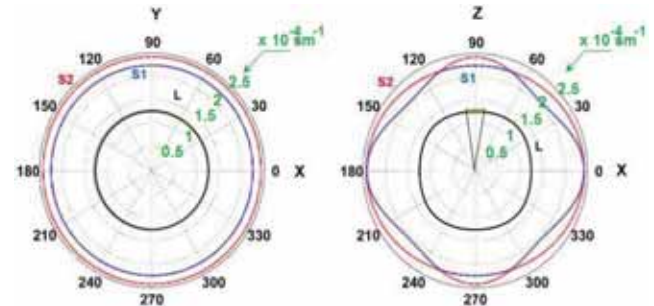


Fig. 6. Calculated slowness curves for GaN for in-plane and out-of-plane acoustic wave propagation. The green shaded regions indicate the slowness values extracted from the frequency of resonators fabricated at UM and [16], [17], [57]–[61]. The measured velocities match well with theoretical estimates.

in the domain of high-power and high-frequency operation (See Table IV) [6], [52], [53].

It is worth noting that more recently InAlN was proposed to replace AlGaIn as the barrier material. Due to the high polarization of AlN and InN components of the barrier, even higher carrier densities can be obtained using InAlN [54].

G. Acoustic Properties of GaN

As a hexagonal piezoelectric material, GaN can be used to demonstrate acoustic transducers. While conventional acoustic transducers use very strong bulk ferroelectrics for actuation on the macro-scale (for applications such as sonar and ultrasound), there is a growing trend for using materials such as thin-film PZT and AlN in micro-acoustic implementations, such as piezoelectric micro-machined ultrasonic transducers (pMUTs) [55], [56]. GaN can be a very attractive option for high output power, high-frequency capable acoustic transducers, with the added advantage of co-fabrication and integration with the necessary drive and control electronics. The slowness curves for GaN (inverse of acoustic velocity) as a function of propagation vector for both in-plane and out-of-plane modes can be calculated based on the stiffness matrix described in Section II.C (Fig. 6). For a majority of resonant devices described in this review, the mode of operation depends on longitudinal waves trapped in a mechanical resonant cavity. The values for extracted acoustic velocity from these resonant devices match the expected longitudinal velocities in plane (7960 m/s) and along the c-axis (8044 m/s). Extracted longitudinal velocities for a number of GaN resonators fabricated

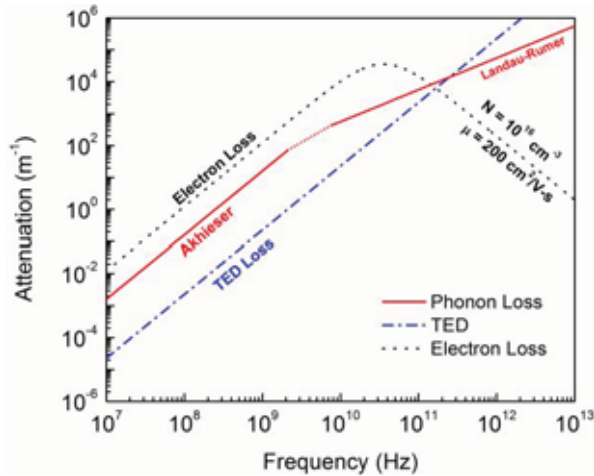


Fig. 7. The calculated intrinsic attenuation for acoustic waves in GaN due to different mechanism. The total attenuation in any given GaN acoustic device is the sum of these losses along with extrinsic losses that are dependent on design and operating conditions. The attenuation due to electron scattering in GaN is highly dependent on the free electron concentration and the mobility.

at UM and [16], [17], [57]–[61] lie in the range of 7200 m/s to 7800 m/s. Slight deviations from the exact theoretical velocity values could be attributed to the effect of a small tilt of the c -axis of the manufactured thin films, and the loading due to metal electrodes and buffer layer on the real devices. The mass density is assumed to be 6150 kg/m³ in all calculations.

The longitudinal velocities of GaN (both in-plane and out-of-plane) are very similar to that of crystalline Si (Table I). In the popular thin-film piezoelectric-on-Si (TPoS) configuration [62]–[65], the use of GaN as the transduction layer on Si (as opposed to using AlN for example) has the potential to reduce acoustic loss, as acoustic velocities of GaN and Si are very similar.

Acoustic waves travelling through GaN, like any other elastic material, is attenuated via a number of intrinsic scattering processes. A comprehensive knowledge of the loss sources and mechanisms is crucial to designing highly sensitive and energy efficient electromechanical devices. Most important among scattering processes are the anharmonic phonon-phonon scattering (also known as phonon loss), loss due to thermoelastic damping (TED loss), and phonon-electron loss due to piezoelectric coupling or deformation potential coupling [15]. Each loss mechanism is dependent on the material properties and dimensions of propagating path in the GaN film, as well as the frequency of the acoustic wave. The analytic expressions for these mechanisms are given by Eqns. (1–4), and representative indication of the losses is provided in Fig. 7 as a function of frequency.

$$\alpha^{pp} = \begin{cases} \frac{C_v T \gamma^2 \tau}{2 \rho s^3} \left(\frac{\omega^2}{1 + \omega^2 \tau^2} \right) & \text{for } \omega \tau < 1 \\ \frac{\pi^5 \gamma^2 k_b^4 T^4}{30 \rho s^6 h^3} \omega & \text{for } \omega \tau > 1 \end{cases} \quad (1)$$

$$\alpha^{TED} = \frac{\kappa T \beta^2 \rho}{18 C_v^2 s} \omega^2 \quad (2)$$

TABLE V
MATERIAL PROPERTIES USED FOR CALCULATION OF ACOUSTIC LOSS COMPONENTS OF WURTZITE GaN

Material Property	Values	Units	Ref.
ρ (mass density)	6150	kg/m ³	[6]
C_s (specific heat)	490	J/kg-K	[6]
μ (electron mobility (bulk GaN))	200	cm ² /V-s	[6]
N (free electron concentration)	1×10^{16}	cm ⁻³	-
K (piezoelectric coupling coefficient)	0.02	-	-
ϵ_r (dielectric constant of GaN)	9.5	-	[6]
τ (phonon relaxation time)	2.02×10^{-12}	s	-
κ (thermal conductivity)	130	W/m-K	[6]
β (coefficient of linear expansion)	5.6×10^{-6}	K ⁻¹	[6]
s (acoustic velocity)	8000	m/s	[6]
γ (Grüneisen parameter)	1.18	-	[66]
Ξ (deformation potential constant)	12	eV	[67, 68]
τ_R (intervalley relaxation time)	1.2×10^{-12}	s	[69]

$$\alpha^{DP} = \frac{N \Xi^2}{9 s^4 k_B T \rho} \frac{\omega^2 \tau_R}{1 + \omega^2 \tau_R^2} \quad (3)$$

$$\alpha_{SW}^{pe}|_{n=0} = \frac{k^2}{2s} \frac{w_c}{1 + \left(\frac{w_c}{w} + \frac{w}{w_D}\right)^2} \begin{cases} w_c = \frac{\sigma}{\epsilon_0 \epsilon_r} = \frac{q_e \mu N}{\epsilon_0 \epsilon_r} \\ w_D = \frac{s^2 q_e}{\mu k_B T} \end{cases} \quad (4)$$

Table V provides a summary of the material properties used in the calculations [15]. The intrinsic losses are described by the attenuation coefficients = α^i (attenuation per meter), where the superscript i refers to the specific attenuation mechanism. Other terms used in these equations are the angular frequency ω (rad/s), absolute temperature T (K), permittivity of free space ϵ_0 , Boltzmann's constant k_B , and Planck's constant h . Calculations are carried out for room temperature conditions.

It is to be noted that the phonon-electron attenuation mechanisms are reversible under certain conditions and can be converted to a phonon-electron gain. This analysis and experimental verification has been detailed elsewhere [15], [16], [70]–[73], and is out of the scope of the present work. Other intrinsic losses are based on the defect density of the film and losses at the interface of GaN and other materials. In a practical device, anchor losses and viscoelastic losses may also be present depending on the device design and operational conditions, but these are extrinsic losses and not solely dependent on the material itself.

III. GROWTH AND PROCESSING TECHNOLOGY

A. GaN Epitaxial Growth

There are numerous studies on the epitaxial growth techniques and optimization of GaN, which are out of the focus of this review [74]–[76]. MBE and MOVPE/MOCVD are the two common techniques for the growth of GaN on Si that is used in MEMS applications. The threading defects in GaN are dislocation lines normally oriented parallel to the c -axis of the material, with reported densities of $10^8 \sim 10^{11}$ cm⁻². Most of them have a Burgers vector with an edge component (mixed or pure edge-type dislocations). Pure screw-type threading dislocation densities of less than 10^7 cm⁻² can be obtained for GaN-on-Si substrates [77], [78]. Edge type dislocations and point defects can become charged and act as centers

of Coulomb scattering, whereas screw-type dislocations have been reported to cause electrical leakage, causing degradation in electric and optoelectronic performance as well as long-term reliability [79]. However, the measured acoustic properties of GaN suggest that the issue is less significant in the case of mechanical and acoustic properties of GaN.

B. Fabrication of GaN Suspended Microstructures

GaN in particular and group III-nitrides in general are notable for their excellent chemical stability as characterized by their invulnerabilities to wet etching. No wet etching technique has been reported to date for effective removal of single crystalline GaN. To realize suspended microstructures, a sacrificial layer can be deposited/grown and selectively removed later. However, single crystalline GaN can only be easily grown on single crystalline materials which are also hard to remove. Due to difficulties in removal of the sacrificial layer on which GaN can be grown, the most practical option for releasing GaN structures for MEMS is the selective removal of the substrate under the GaN device area. In this case, Si is the best candidate as the substrate since mature micromachining techniques can be employed to either isotropically etch Si from the front-side (*e.g.*, using xenon difluoride (XeF₂)) or through deep reactive ion etching (DRIE) process from the back-side of the wafer. Some of the most commonly used etching techniques of GaN are briefly discussed below.

1) *Wet Chemical Etching*: Various wet etchants for GaN have been investigated, including aqueous mineral acid and base solutions, and molten salts; however, the optimum etching parameters are highly dependent on crystal quality, orientation, polarity, and material properties (Fig. 8).

Aqueous KOH between 26 °C and 80 °C has been shown effective only for etching MBE-grown N-polar GaN crystals. Etching produced triangular-shaped pyramids for N-polar GaN crystals and no effect on Ga-polar GaN crystals under the same conditions [80]. Similar results have been reported for hot Phosphoric acid (with temperature > 200 °C), where only defect areas are etched on the Ga-polar GaN crystals, and show hexagonal etch pits with an etch rate of ~1 μm/min for MOCVD-grown GaN. No significant etching was observed for temperatures lower than 160 °C [81], [82].

Although not very effective for patterning GaN, wet etching could be an important device fabrication process that complements dry etching techniques. Due to the strong physical nature of dry etching, it results in low etch-selectivity between materials, and subsurface damage by ion bombardment. In contrast, wet etching, produces negligible damage, can be highly selective, is relatively inexpensive with higher throughput, and can be done with simple equipment. Besides patterning of GaN, some other applications of wet etching include surface treatment, defect decoration, polarity identification by producing characteristic pits or hillocks, and device fabrication on smooth surfaces [83].

2) *Photoelectrochemical (PEC) Etching*: Due to the limitations of wet chemical etching of GaN, many groups investigated the stimulation of etching by external injection of photo-generated holes to oxidize Ga atoms. The oxidation

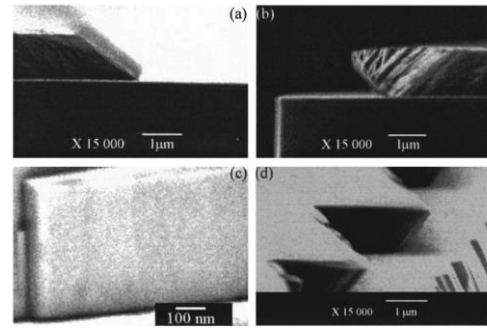


Fig. 8. Scanning electron microscope (SEM) images of crystallographic surfaces of GaN made by wet etching. (a) {1013}Plane etched by H₃PO₄. (b) Undercut {1012}plane etched by H₃PO₄. (c) Vertical {1010}plane etched by KOH in ethylene glycol. (d) Undercut {1011}plane etched by molten KOH [87].

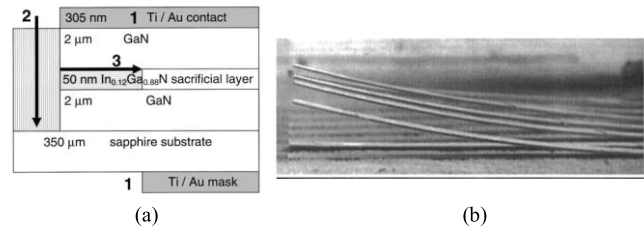
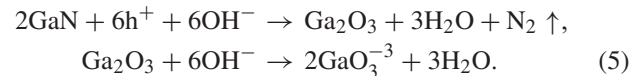


Fig. 9. (a) GaN/InGaN/GaN stack, where InGaN is used as the sacrificial layer to form suspended microstructures. (b) SEM images of the released cantilever structures curved upwards by the relief of intrinsic strain gradient. After [85].

process requires holes that can be generated by light with photon energy larger than the band gap of GaN [83]. The oxidation and removal process is summarized in the two-step chemical Eq. (5) [2]:



The first PEC etching of GaN was demonstrated by Minsky *et al.* [84] using a He–Cd laser with a wavelength of 325 nm and light intensities of 570 mW/cm². The etch rates were about 400 and 40 nm/min in KOH and HCl solutions, respectively. Selective PEC etching can also be used to form suspended structures by selective removal of III-nitride-based crystalline sacrificial layers. The techniques used for selective PEC etching include bandgap selective, dopant selective, or defect selective PEC etching. Bandgap selective PEC etching is particularly used for fabrication of suspended GaN structures. In [85], InGaN is used as sacrificial layer in InGaN/GaN hetero-structures, where a laser with excitation energy larger than InGaN bandgap ($E_g = 3.0$ eV) and smaller than GaN bandgap ($E_g = 3.4$ eV) is used to generate holes that can only oxidize the InGaN layer. Therefore, the InGaN layer is etched, while the GaN layer is left intact (Fig. 9).

Unlike GaN chemical etching, PEC etching can be done at room temperature and is not polarity selective. Furthermore, ion bombardment and surface damage associated with dry etching is eliminated with this technique [86].

3) *Plasma Dry Etching*: Currently, plasma-based chemical dry etching is the most commonly used patterning technique for group III-nitrides. The mechanisms and variations have

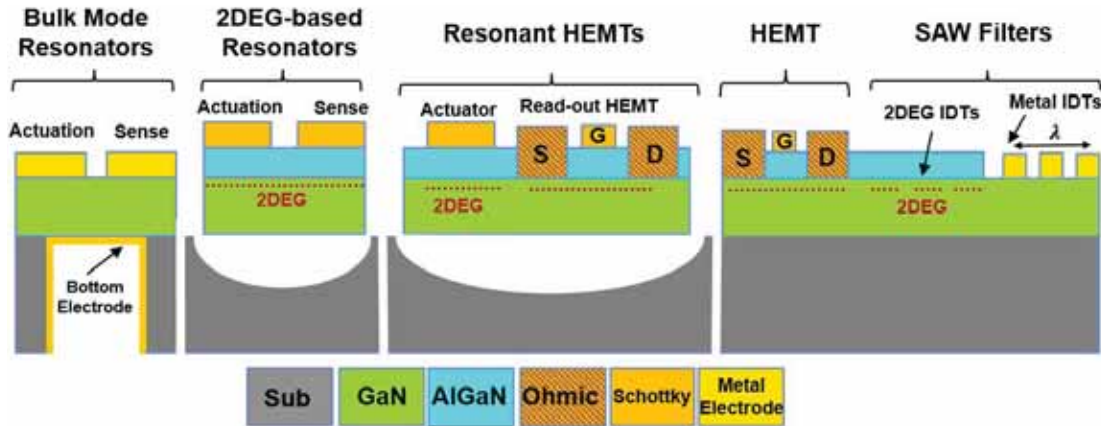


Fig. 10. A cross-section schematic demonstrating various types of electromechanical devices that can be manufactured using GaN thin films grown on Si substrates. Functionally, these systems can act as sensors, readout circuitry, amplifiers, and communication nodes. Two or more of these device types can potentially be integrated or co-fabricated on the same substrate, imparting GaN-based systems a range and versatility rivaling Si. This concept can be extended to GaN films grown on SOI substrates.

TABLE VI
PROCESS PARAMETERS FOR ICP ETCHING OF GaN

Parameter	Unit	Value
Chamber Pressure	mTorr	5 -10
Cl ₂ Flow rate	sccm	24-36
BCl ₃ Flow rate	sccm	6-10
Ar Flow rate	sccm	5-8
He Pressure (wafer back-side cooling)	Torr	8
ICP Power	W	500
RF Bias Power	W	50-100
Etch Rate (anisotropic)	nm/min	~200

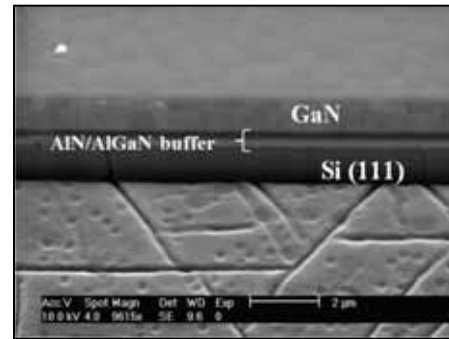


Fig. 11. A SEM image of a GaN thin film etched using ICP process, with the parameters given in Table VI, resulting in smooth and vertical sidewalls. This image shows the AlN/AlGaIn buffer layers and the Si substrate deliberately over-etched to clearly distinguish the GaN film. The crack and defect patterns on the etched Si are a result of micromasking and pattern transfer from the AlGaIn buffer layer as it is etched down. Image is at 45° tilt.

been reviewed in detail by Pearton *et al.* [88]. Reliable, well-controlled patterning can be achieved by a variety of dry etch platforms. In particular, high-density electron cyclotron resonance (ECR) and inductively coupled plasma (ICP) etch processes have yielded smooth, highly anisotropic, etch characteristics. Etch rates that can exceed 1.0 $\mu\text{m}/\text{min}$ can be achieved. Halogen-based plasma chemistries (Cl-, I- and Br-based plasmas) yield high-quality etch characteristics. The choice of the reactive source gas (Cl₂, BCl₃, ICl, IBr, *etc.*) and secondary gases (H₂, N₂, Ar) changes the concentration of reactive neutrals and ions in the plasma, which directly correlates with the etch rate. Smooth, anisotropic pattern transfer was obtained over a wide range of plasma etch platforms, chemistries, and conditions. Fast etch rates, high resolution features, and low damage are obtained when the chemical and physical components of the etch mechanism are balanced.

The process parameters used for anisotropic etching of GaN by the UM group in [16], [17], [57], [61], and [89]–[92] are shown in Table VI. This process results in smooth and vertical sidewalls (Fig. 11). As expected, increasing gas flows within a range increases the isotropicity of the etching process.

4) *Thin Film Transfer*: A unique, non-conventional approach to realizing GaN thin films on substrates that are not best suited for epitaxy is the wafer transfer method. This method involves growing GaN on sapphire, SiC, or Si (111) parent substrates, bonding the film to a new host substrate (with the GaN film sandwiched in between), and cleaving the bonded pair using a separation technique. Note

that the host substrates such as Si (100) and glass [93] are not amenable to GaN epitaxy. The separation techniques include laser liftoff [94], [95] and splitting the interface by first weakening it by ion implantation [96]. These studies have shown that the quality of the transferred films is almost as good as the original epitaxially grown film and can meet GaN LED wafer standards. GaN HEMTs with good characteristics have been demonstrated on a host Si (100) substrate [97]. While this is a relatively new technique, wafers made with transferred GaN films are now being offered by commercial GaN manufacturers [98].

IV. GaN MICROELECTROMECHANICAL DEVICES

Based on the epitaxial growth and thin film processing technologies discussed above, a variety of GaN MEMS and devices can be fabricated using GaN-on-Si substrates. The ability to etch the Si substrate easily and selectively using isotropic or anisotropic, wet or dry etching methods offers advantages beyond the difficult-to-machine sapphire or SiC substrates. A general schematic shown in Fig. 10 demonstrates versatile devices that can be implemented using GaN-on-Si substrate. The most popular electromechanical devices that

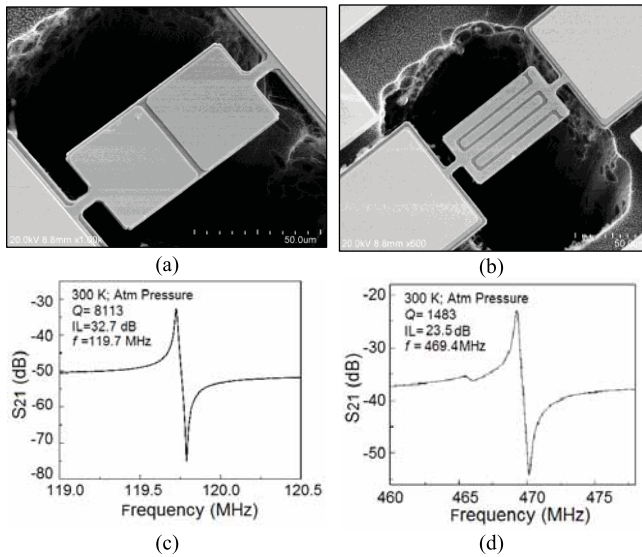


Fig. 12. Representative SEM images (a, b) and RF transmission responses (c, d) of length-extensional mode GaN resonators. These devices work efficiently in the VHF and low-UHF range and can be used for timing and sensing applications. Multiple frequencies are possible on a single substrate.

have been implemented thus far using GaN-on-Si wafers are micromechanical resonators and cantilevers. In the following subsections, we review a number of GaN-based devices reported in the literature. In Section V, we extract some of the intrinsic properties of GaN (grown on Si) from the data presented in this section.

A. Piezoelectric Actuation & Readout

Bulk acoustic wave (BAW) resonant devices made from GaN have relied heavily on the piezoelectric properties of the material for actuation and readout. Piezoelectrically actuated GaN resonators operating in various modes of resonance and across a broad range of frequencies have been demonstrated by a number of research groups in the recent past. Popular implementations of such devices are length- or width-extensional resonators and thickness-mode resonators.

1) *GaN Length-Extensional Mode Resonators*: Length-extensional mode GaN resonators are mechanically released GaN plates tethered at specific nodal points. They are actuated by using the e_{31} coefficient of GaN by applying an RF signal across the thickness of the GaN film, causing longitudinal vibrations in the frequency determining dimension (length or width). The distinct advantage of in-plane length-extensional mode resonators is that the significant dimension (and thus the resonant frequency) can be set lithographically, enabling multiple fundamental vibration modes on a single substrate. Furthermore, the resonators can be operated at higher harmonics by using inter-digitated transducer (IDT) top electrodes (Fig. 12). Length-extensional mode GaN resonators have been demonstrated in the recent past, with frequencies in the VHF and low-UHF range from 4 MHz to more than 400 MHz [17], [57], [90], [99], [100].

2) *GaN Thickness-Extensional Mode Resonators*: As with length-extensional mode resonators, thickness-extensional

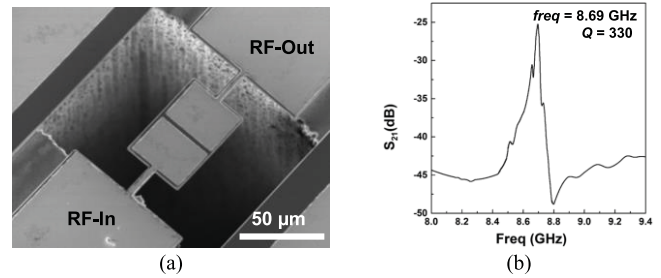


Fig. 13. (a) SEM and (b) de-embedded frequency response of thickness-extensional mode resonator, with a fourth-order thickness mode resonance frequency of 8.69 GHz, exhibiting a Q of 330. Resonance frequency is set by the film thickness. These devices are generally designed to achieve higher frequencies in the high-UHF to SHF spectrum [101].

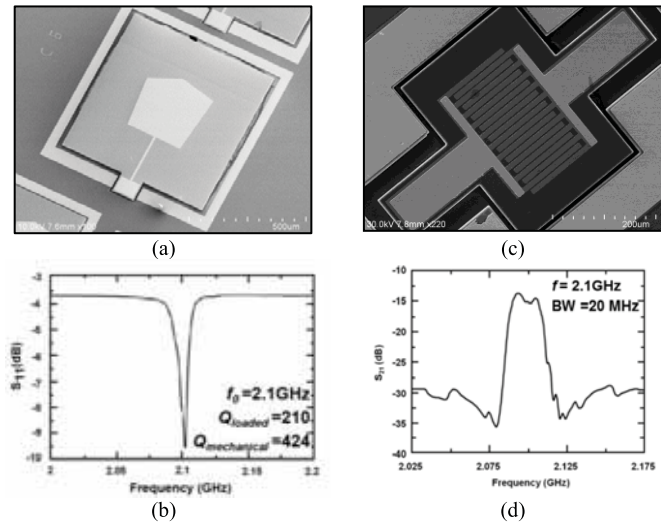


Fig. 14. Similar to the GaN thin-film resonators, one can use GaN-on-Si composite structures to develop TPoS resonators. These resonators combine the robustness and low acoustic loss of a thick Si layer with the efficient piezoelectric actuation of GaN. One can design FBAR type (a, b) or IDT type (c, d) filters using a GaN TPoS structures [89].

mode resonators are longitudinal BAW devices. The fundamental resonance frequency is inversely proportional to the film thickness and the effective piezoelectric coefficient is the larger e_{33} value. With GaN thin-films ranging from less than 1 μm to about 2 μm , resonators with frequencies up to 8.7 GHz have been realized (Fig. 13) [101].

3) *GaN-on-SOI Resonators*: Both thickness-extensional mode and length-extensional mode resonators can be fabricated using GaN-on-SOI substrate in a (Fig. 14) TPoS configuration [63], [64]. Composite resonators have the advantage of combining the piezoelectric properties of GaN with the acoustic properties of the substrate. In general, the thicker composite stack allows for a more mechanically and thermally robust device. If the substrate layer is well doped Si, it can act as the bottom electrode. This eliminates the need for a metal electrode with a large acoustic mismatch with GaN. The use of GaN-on-SOI substrates can be explored in the future for heterogeneous integration of GaN- and Si-based electromechanical devices and readout/signal processing circuitry on the same substrate.

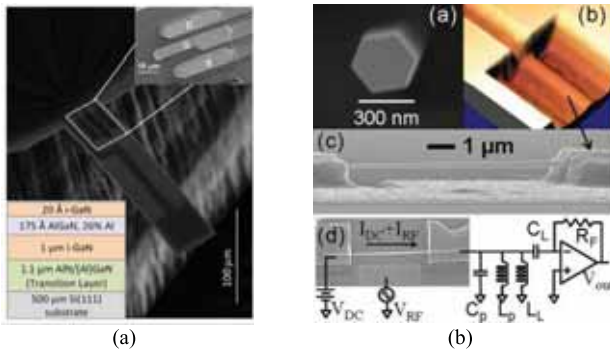


Fig. 15. (a) GaN cantilever structures (From [103]) and (b) GaN nanowires (From [107]) can be used as sensing elements utilizing the piezoresistive effect in AlGaIn/GaN 2DEG sheet. The high gauge factor of AlGaIn/GaN is due to the large modulation of the electronic properties of GaN and AlGaIn due to strain. Another major advantage of GaN piezoresistors is the ability to work at significantly elevated temperatures and still retain a high sensitivity.

B. Piezoresistive Sensing and Readout

Mechanical devices based on the GaN/AlGaIn system can be used as highly sensitive piezoresistive sensors for detecting small amounts of static or dynamic strain [102]–[105]. Strain applied to mechanically released, flexural-mode micro-cantilevers modulates the piezoelectric polarization at the GaN/AlGaIn interface [104] as well as the carrier mobility due to strain-induced band-bending [105], [106]. Both effects lead to large detectable changes in the instantaneous resistance. These changes can be sensed by simple readout circuits or by using an integrated 2DEG-based transistor (Fig. 15(a)). Gauge factors (the relative change in resistance with respect to change in strain) as high as 3532 [103] have been reported for such structures. This is in comparison to the significantly lower numbers reported for Si [103]. GaN/AlGaIn piezoresistive systems are expected to maintain high gauge factors even at elevated temperatures, beyond the working range of conventional semiconductor piezoresistors, thus making them attractive candidates for harsh environment sensing. The piezoresistive effect has also been used as a readout mechanism for GaN nanowire based mechanical resonators (Fig. 15(b)) [107].

C. 2DEG Electrodes

As mentioned earlier, a 2DEG sheet is induced at the AlGaIn/GaN interface due to the spontaneous and piezoelectric polarization. The origin of 2DEG, unlike the conducting channel in Si transistors, suggests that they are very sensitive to mechanical stress, changing the piezoelectric polarization-induced surface and interface charges. Furthermore, 2DEG is sensitive to other environmental influences, such as temperature, illumination, or chemical surface modifications. Since the 2DEG is formed very close to the surface (typically ~ 30 nm below the surface), it is highly sensitive to surface potentials. 2DEG has been shown in sensor applications such as pH, viscosity, mass, and a variety of other novel sensor concepts are conceivable based on its properties. Moreover, 2DEG can replace metal electrodes in piezoelectric resonators. 2DEG conductive sheet, inherent to the AlGaIn/GaN piezoelectric

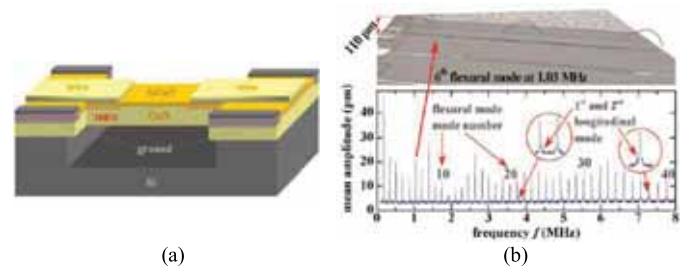


Fig. 16. (a) Schematic and (b) frequency response of a piezoelectrically actuated AlGaIn/GaN resonator using 2DEG as the bottom electrode [110].

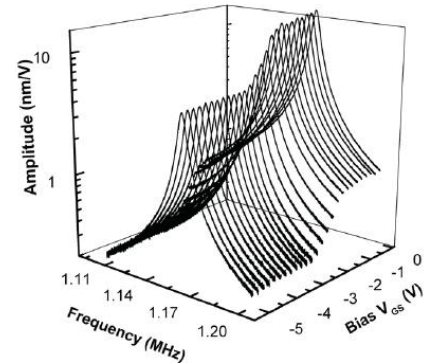


Fig. 17. Actuation efficiency versus bias voltage of an AlGaIn actuator where a 2DEG is used as bottom electrode. After [111].

material system can effectively reduce the metal loading and acoustic mismatch associated with metal electrode deposition, and thus improve the resonator performance. It can either be utilized as the top or bottom electrode in MEMS for actuation as well as readout. A summary of GaN-based resonant devices with embedded 2DEG electrodes, as well as a class of resonant devices, *i.e.* “Resonant HEMTs,” based on 2DEG sensing is provided in the following subsections.

1) *2DEG Bottom Electrode*: The 2DEG at the AlGaIn/GaN-interface can be utilized as the bottom electrode for piezoelectric actuation and read-out of AlGaIn/GaN suspended beams (Fig. 16). The elimination of bottom electrode metallization is particularly beneficial in GaN-based resonators since single crystalline GaN cannot be directly grown on metal sheets. Implementation of 2DEG as the bottom electrode was demonstrated in [100] and [108]–[110], where resonant frequencies of up to 60 MHz with a maximum frequency times Q ($f \times Q$) value of 9.42×10^9 have been reported for longitudinal- and flexural-mode resonators.

The main difference between using metal-piezo-2DEG instead of the known metal-piezo-metal structures is that in the case of 2DEG the actuation amplitude is bias dependent and drops below the pinch-off voltage [111] (Fig. 17). Nevertheless, the actuation remains non-negligible at lower negative biases. This is due to the remaining field distribution inside the piezoelectric GaN buffer.

2) *Patterned 2DEG as Top Electrode*: In order to reduce the mass loading associated with the deposition of metal as the top electrode on piezoelectric resonators, several approaches have been taken. In AlN piezoelectric resonators,

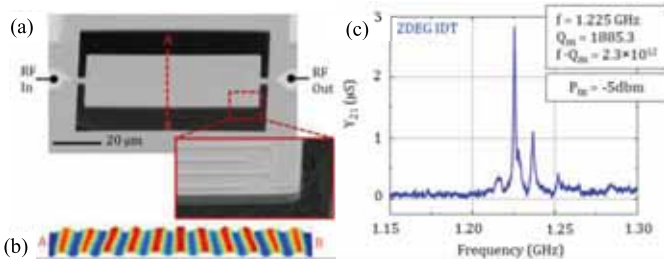


Fig. 18. (a) A SEM of 2DEG IDT resonator. The 2DEG electrodes are patterned with a 90 nm deep AlGaIn etch. (b) Mode shape showing the strain fields induced at resonance. (c) De-embedded frequency response of 1.22 GHz 2DEG IDT resonator. After [58].

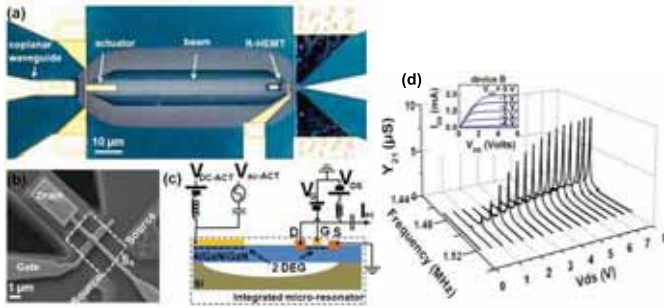


Fig. 19. (a) optical image, (b) a SEM image, and (c) measurement setup of a flexural-mode Resonant HEMT. (d) Amplification of mechanical transduction inside the HEMT integrated on the flexural beam [115].

efforts have included physically separating electrodes from the piezoelectric thin film [112] and segmentation of IDT metal electrodes [113]. GaN material systems benefit from the 2DEG conductive sheet, which can be used to define electrodes and thus completely remove metal from the resonant structure. In [58], a metal-free piezoelectric resonators is presented, which utilizes 2DEG IDTs to drive acoustic waves in an AlGaIn/GaN hetero-structure (Fig. 18). Metal-free acoustic filters, with patterned 2DEG electrodes had been previously reported in AlGaIn/GaN SAW filters discussed in Section E.

D. AlGaIn/GaN Resonant HEMTs

Resonant AlGaIn/GaN HEMTs exploit the high sensitivity of the HEMT 2DEG conducting channel to the acoustic strain induced by an actuator in a resonant cavity on which the HEMT is fabricated. As mentioned earlier, the 2DEG sheet is very sensitive to mechanical stress. A small change in stress translates into a considerable change in 2DEG carrier concentration, which is in turn sensed through the change in the HEMT drain current. 2DEG sensitivity to mechanical stress has been widely used in static AlGaIn/GaN strain sensors and discussed in detail in the literature [114]. In the resonant HEMTs, the acoustic wave is launched into the resonant device, for example by an additional Schottky contact for piezoelectric excitation, and sensed through detection of a peak in the frequency response of the HEMT drain current at resonance. Using HEMT-based read-out, capacitive feed-through is reduced allowing for operation at higher frequencies. Also higher sensitivity and signal amplification is achieved due to

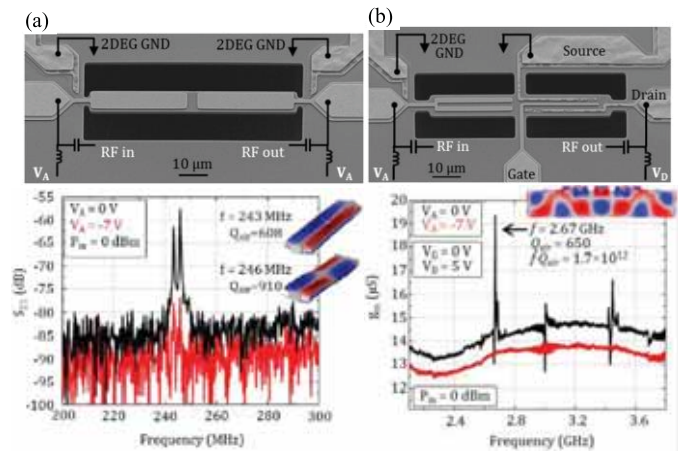


Fig. 20. (a) (Top) SEM image and (bottom) measured frequency response of a passive resonator in air. (b) (Top) SEM image and (bottom) frequency response of a piezoelectric drive, HEMT-sensed resonator [59].

inherent gain in the HEMT. Resonant HEMTs are discussed in the next section and categorized by their mode of resonance, *i.e.* flexural, longitudinal, and thickness mode. They are all fabricated on GaN-on-Si substrates.

1) *Flexural-Mode Resonant HEMTs*: AlGaIn/GaN resonant HEMTs were first demonstrated in [115], where flexural mode acoustic resonance was excited and sensed on a doubly clamped beam using Schottky diodes for excitation and HEMT transducers for read-out (Fig. 19).

Working at 1.49 MHz with a Q of 1850, the device was operated at different drain and gate biases. This enabled the observation of intrinsic amplification of the mechanical transduction (Fig. 19). Moreover, a detailed study based on the same kind of devices [113] confirmed that the response is driven by the 2DEG mobility under the gate and in the access regions. A quantitative model was proposed to account for the transconductance variations that have strong similarities with transconductance curves usually recorded on such transistors.

2) *Width-Extensional Mode R-HEMTs*: Bulk acoustic width-extensional mode resonant HEMTs have been reported in [59] and compared with passive AlGaIn/GaN resonators using 2DEG as the bottom electrode. Resonance frequencies ranging from 240 MHz to 3.5 GHz with Q values of up to ~ 500 are reported in air. Fig. 20 compares a passive AlGaIn/GaN resonator with a width-extensional resonator readout using an active HEMT. In Fig. 20(a), the HEMT provides electromechanical amplification of the mechanical signal, enabling sensing at much higher frequencies than possible with passive devices.

3) *Thickness-Extensional Mode R-HEMTs*: A multi-gigahertz thickness mode AlGaIn/GaN resonant HEMT is reported in [61] and [91], where the vertical electrical field excites the thickness-mode acoustic resonance of a resonating stack through the thickness-mode piezoelectric coefficient (e_{33}). Acoustic signal is excited through a back gate Schottky contact and read-out by measuring the drain current of the sense HEMT. The back gate and the sense HEMT channel are placed at locations under maximum strain. The source is placed at a nodal point and tied to GND.

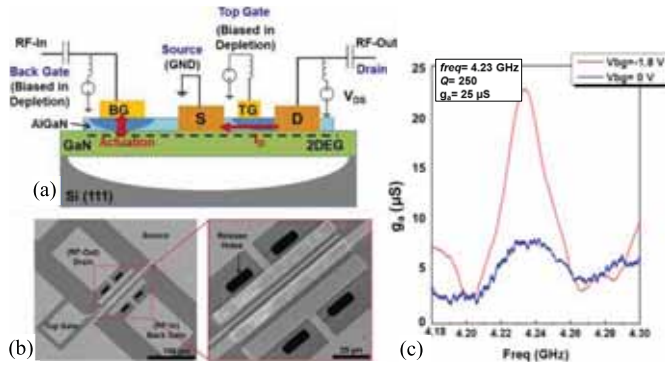


Fig. 21. (a) Schematic view of an AlGaIn/GaN thickness-mode resonant HEMT. AC signal is applied to the back gate that is biased in the depletion region and picked up by sensing the drain current. (b) SEM images of the fabricated device. (c) Measured acoustic transconductance, showing a resonance peak only when the actuator is biased in depletion [91].

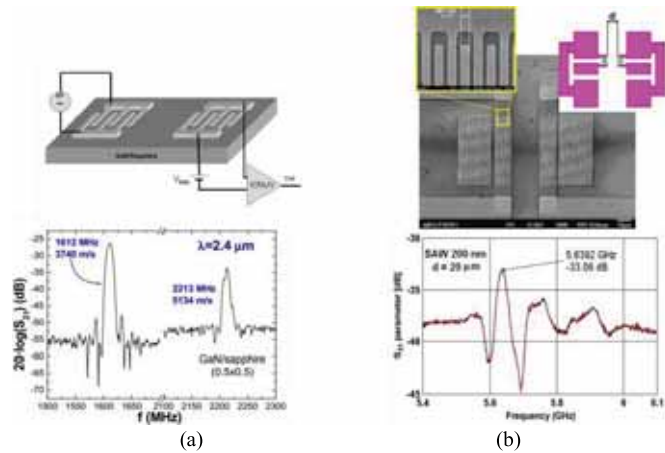


Fig. 22. (a) Schematic and transmission response of GaN-on-sapphire SAW filter, after [117]. Two peaks are observed in the 0-3 GHz frequency range, at 1.6 GHz and 2.2 GHz, associated with Rayleigh and Love waves respectively. (b) SEM images and transmission response of GaN-on-Si SAW filters, with 200 nm spacing ($\lambda = 0.8 \mu\text{m}$), and a 5.6 GHz resonance frequency [118].

The device shows the second-order resonance frequency of 4.23 GHz with a Q of 250 (Fig. 21). The acoustic transconductance (g_a) rises to $\sim 25 \mu\text{S}$ when the transducer is ON. Co-integrated with GaN ICs, this resonant HEMT can potentially offer all-GaN integrated nano/micro sensors and systems. The resonance frequency can be further increased by exciting higher harmonics of the thickness-mode resonance. This device exhibits the highest resonance frequency reported thus far for a resonant HEMT.

E. SAW Filters

SAW devices have been traditionally fabricated on quartz, ZnO, LiTaO₃, and LiNbO₃ [116] and used in a variety of sensing and communication applications. The III-nitride family combines a high SAW velocity and electromechanical coupling coefficient with excellent thermal and chemical stability. All these properties are of high interest for the development of SAW devices operating at frequencies higher than 1 GHz, a common requirement of most modern telecommunication applications [117].

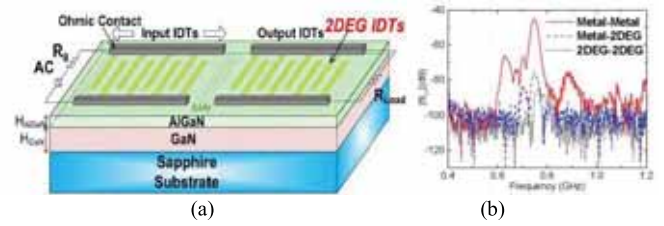


Fig. 23. (a) Schematic of the SAW filter with 2DEG IDTs on AlGaIn/GaN/Sapphire structure. (b) Frequency responses of the SAW filters with metal-metal, metal-2DEG, and 2DEG-2DEG IDTs [119].

In [117], SAW filters with resonant frequencies of up to 2.22 GHz were realized on GaN-on-sapphire substrate, with 600 nm wide fingers and inter-digit spacing (Fig. 22(a)). More recently, a 5.6 GHz SAW filter, with 200 nm wide fingers and inter-digit spacing was realized on GaN-on-Si substrate (Fig. 22(b)), marking the highest resonance frequency achieved for GaN SAW resonators to date [118].

SAW filters using 2DEG IDT on AlGaIn/GaN heterostructure are demonstrated in [119] based on a fluoride-based (CF₄) plasma treatment technique. The CF₄ plasma treatment is used to pattern 2DEG IDT on a planar surface without removing the top AlGaIn layer (Fig. 23(a)). SAW peaks correspond to the Rayleigh and pseudo-bulk modes of the epitaxial structure. The Rayleigh mode is primarily confined to the thin-film epitaxy, while the pseudo-bulk mode is primarily confined to the sapphire substrate near its interface with GaN. The frequency range of the fabricated SAW filters is between 400 MHz and 1.2 GHz (Fig. 23(b)).

In [120], 2DEG-based SAW filters are integrated with HEMT structures to study the emission of SAWs by AlGaIn/GaN HEMTs under certain bias conditions. IDT-IDT and HEMT-IDT pairs are compared for SAW emission and detection. Integrated HEMT-IDT structures can enable real-time evaluation of epitaxial degradation as well as high-speed, amplified detection of SAWs.

F. Integrated Circuits With MEMS Resonators and HEMTs

GaN microsystems take advantage of integration of GaN mechanical components with GaN HEMTs. As mentioned earlier, GaN HEMTs are being widely used in RF power amplifiers. There is a great demand for miniaturization of such products and designers continuously move from hybrid (circuit board with discrete components) to integrated (single, small chip) more compact solutions. Integrated microsystems offer higher densities, added functionality, and suffer less from parasitics associated with wire-bonding or other hybrid solutions. One of the applications of integrated GaN material systems is MEMS-based oscillators. MEMS oscillators are critical in building all-integrated accurate timing references and frequency-stable circuits. Low phase noise, temperature stable MEMS oscillators operable at harsh environments with high resonance frequencies and significant delivered output powers are achievable in GaN integrated microsystems. Despite of their great promise, few reports exist on implementation of an all-GaN oscillator, where a GaN resonator is

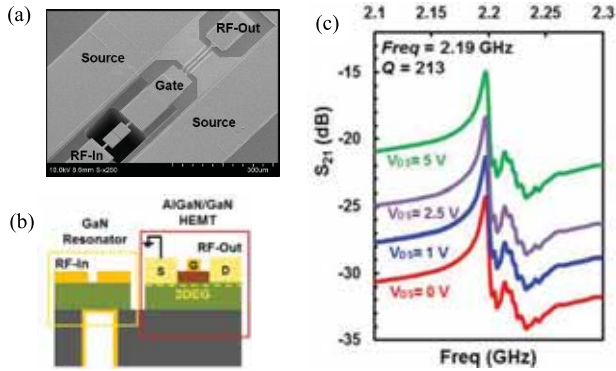


Fig. 24. (a) SEM image and (b) schematic, (c) frequency response of integrated cascade of a resonator and HEMT. The insertion loss is modulated by more than 10 dB [60].

utilized for frequency selectivity and an AlGaIn/GaN HEMT provides gain for building up oscillation. Below, we review the two recent structures that integrated GaN resonators and AlGaIn/GaN HEMTs.

1) *Integrated Bulk-Mode GaN Resonators and HEMTs*: In [60], a platform for monolithic integration of GaN BAW resonators and HEMTs is shown (Fig. 24). The output port of the resonator is connected to the gate of the transistor, where the signal gets amplified by the intrinsic gain of the transistor and picked up at the drain. This platform provides the main building block of a Pierce oscillator circuit, where the feedback loop is formed by simply connecting the resonator input to the HEMT drain.

2) *GaN SAW Oscillator*: In [121], a SAW device has been incorporated in a feed-back loop with an off-the-shelf amplifier to build an all-GaN oscillator (Fig. 25). The SAW filter shows a Q of 1730 at a resonance frequency of ~ 1 GHz. A phase noise of -115 dBc/Hz was recorded at 10 kHz offset from the carrier with noise floor of -165 dBc/Hz. Several tracks are currently considered to improve the Q of the resonator and hence the phase noise figure of merit.

V. PERFORMANCE METRICS FOR GaN RESONANT DEVICES

A. Quality Factor and $f \times Q$ Limits

One of the most important metrics for mechanical resonators is the product of frequency and Q . The Q of an acoustic resonator is directly related to the total energy lost, which is quantified by the attenuation coefficient, as discussed in Section II-G. While extrinsic energy loss to the ambient media (damping and anchor loss) can be reduced by vacuum packaging and using a good design, energy lost as heat (thermoelastic damping), intrinsic energy losses to the material lattice (phonon-phonon loss), and energy lost to conduction electrons (phonon-electron loss) are considered the ultimate limiting factors of the resonator Q . The measured values of the resonator $f \times Q$ are a good indicator of how close the resonator is to the limiting values. If the acoustic wave is considered as a strain wave in the material, at a frequency that is much lower than the inverse of the lattice relaxation time of the material crystalline structure, it is found theoretically

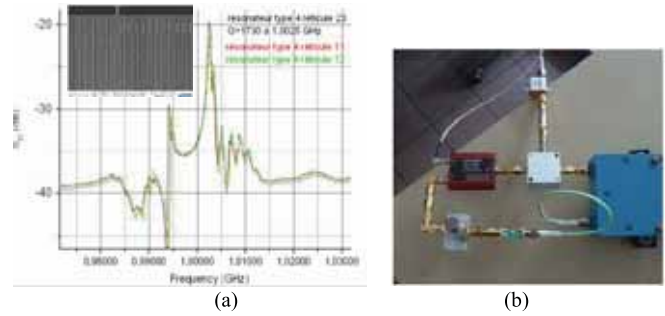


Fig. 25. (a) Frequency response of a double-port SAW resonator. Inset shows the SEM image of the resonator built on GaN-on-Si (111). (b) Experimental oscillator setup, including the packaged resonator, a low noise integrated amplifier, a phase-shifter and a coupler [121].

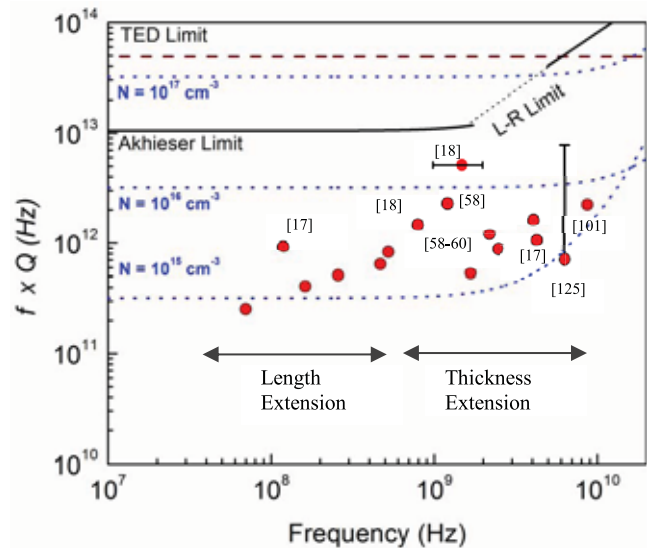


Fig. 26. Calculated values of the $f \times Q$ limits for the dominant intrinsic dissipation mechanisms in GaN. Measured results (with error bar) from [17], [18], [58]–[60], [101], and [125].

that the product of frequency and the limiting material Q remains constant (across frequency) [4]. This is known as the Akhiezer $f \times Q$ limit. For GaN, this regime should be valid for frequencies as high as 5 GHz. Above this value, the system can be treated as an ensemble of phonons and the limiting values of $f \times Q$ is given by the Landau–Rumer (L–R) regime. For high-frequency longitudinal wave resonators made from GaN, the thermoelastic damping is not significant [122], however, it is generally a dominant damping mechanism for lower-frequency flexural-mode resonators [123], [124]. For GaN, a semiconductor, the electron scattering is also a significant loss mechanism and is highly dependent on the free carrier concentration, the carrier mobility and the coupling between the electrical and mechanical domains (due to piezoelectric or deformation potential coupling) [73].

Fig. 26 shows the $f \times Q$ limit of GaN due to different loss mechanisms and compares that to the measured data (red circles) from GaN resonators presented in the previous sections. The gap between the theoretical and measured results is due to other effects that also play a role in damping the device. It can be seen that the measured

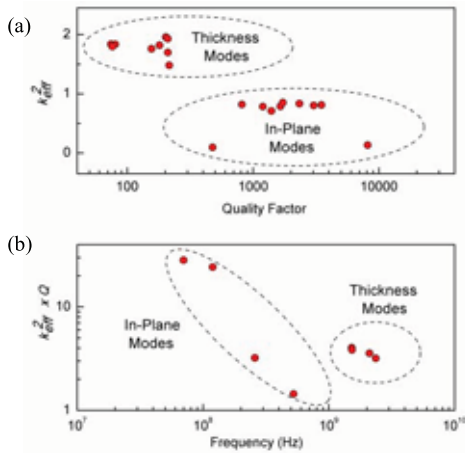


Fig. 27. Measured values of (a) k_{eff}^2 as a function of and (b) $k_{eff}^2 \times Q$ as a function of frequency. Data are taken from prior literature [17], [58]–[60].

$f \times Q$ values are in the same order of magnitude as the maximum possible $f \times Q$ limit even using GaN grown on Si. The exact values are dependent on the quality of the GaN film, the carrier concentration of GaN used, and the specific design of the resonator. However, in general, higher-frequency resonators have shown better performance in terms of $f \times Q$ values.

B. Coupling Efficiency and the $k_{eff}^2 \times Q$ Metric

The piezoelectric coupling coefficient k_t^2 is a material property that determines the efficiency of converting electrical energy into mechanical energy and vice-versa. For the various electromechanical axes of GaN, the values of k_t^2 range from 1.3% for in-plane modes to $\sim 2\%$ for thickness modes [6], [126]. The effective coupling coefficient k_{eff}^2 is extracted from the mechanical response of the resonators and includes the effects of metal electrode loading, non-ideal electrode area coverage, and anisotropic effects [126]. The measured values of k_{eff}^2 in prior literature (Fig. 27(a)) are seen to be close to the calculated maximum values for both the thickness modes (measured to be $\sim 1.9\%$) and in-plane modes (measured to be up to $\sim 0.9\%$).

Another related metric that is used often for characterizing the applicability of a piezoelectric material for use in RF electromechanical filters is the $k_{eff}^2 \times Q$ product. Practically, a higher resonator k_{eff}^2 increases the separation between the series and parallel resonances. For coupled-resonator filter topologies, this higher separation implies a wider bandwidth. A higher Q (for each individual resonator) imparts a sharper roll-off for the filter. Thus, a high $k_{eff}^2 \times Q$ product is desirable for wide-band RF filters [126]. In this regard, measured GaN resonators have demonstrated similar numbers (Fig. 27(b)) in comparison with quartz, diamond, TPoS and Si-based internal dielectric transduction. However, it is significantly lower than stronger piezoelectric materials such as LiNbO₃ [127], or highly optimized devices such as the AlN FBARs [128]. We believe that the consistent and rapid improvements in the reported $k_{eff}^2 \times Q$ of GaN resonators indicate that there is yet room for improvement.

TABLE VII
A COMPARISON BETWEEN RESONANCE FREQUENCY, Q , AND
TRANSCONDUCTANCE (g_a) OF Si AND GaN-BASED
RESONANT TRANSISTORS

Material	Frequency	Q	g_a	Ref.
Si	14.3 MHz	700	-	[129]
Si	71.3 MHz	13200	-	[130]
Si	11.7 GHz	1830	15 μ S	[131]
AlGaIn/GaN	1.3 MHz	226	8 μ S	[132]
AlGaIn/GaN	2.67 GHz	650	6 μ S	[59]
AlGaIn/GaN	2.1 GHz	105	15.5 μ S	[61]
AlGaIn/GaN	4.23 GHz	250	> 25 μ S	[91]

C. Acoustic Transconductance

Acoustic transconductance is a figure of merit specifically used in resonant FET-based sensing, which reflects the changes in the drain current of the transistor, when there is a change in the voltage applied to an actuator. An AC voltage applied to the actuator causes acoustic strain in the resonant structure, which in turn, changes the drain current of the transistor. Therefore, one can define a new transconductance parameter, *i.e.* acoustic transconductance as:

$$g_a = \frac{d(I_D)}{d(V_{BG})}, \quad (6)$$

where g_a is the acoustic transconductance, $d(I_D)$ is the amplitude of the drain AC current and $d(V_{BG})$ is the amplitude of the AC voltage applied to the actuator port (*e.g.*, a back gate Schottky contact). g_a is extracted from the admittance matrix of the resonant HEMT, similar to the extraction procedure of the transconductance of any standard transistor as:

$$g_a = |Y_{21} - Y_{12}| \quad (7)$$

Table VII compares the resonance frequencies, Q s, and the acoustic transconductance values of Si resonant transistors and AlGaIn/GaN resonant HEMTs, extracted from the $|Y_{21} - Y_{12}|$ curves.

D. Temperature Coefficient of Frequency

One of the important metrics for resonator performance is the temperature coefficient of frequency (TCF), which describes the relative shift in the resonator frequency with temperature change. The TCF is a function of the material properties, resonator mode, and dimensions of the device. In most materials, the dominant mechanism is the change in the elastic modulus of the material with respect to temperature, defined by temperature coefficient of elasticity (TCE). For many mechanical resonator applications, such as oscillators, clocks and gyroscopes, the objective is to minimize the TCF in order to get temperature invariant performance. For thermal and infrared (IR) sensors [57], [90], [92], the temperature dependency should be maximized. In both cases, it is important to carefully characterize the TCF of the

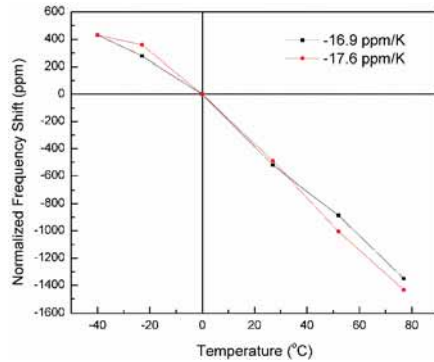


Fig. 28. The change in the frequency of two length-extensional GaN resonators as a function of temperature, showing a negative TCF with experimentally measured values of between -14 ppm/K to -18 ppm/K [16], [17], [89], [90].

resonator. Theoretical calculations for the stiffness coefficients of GaN [133] indicate TCE values of -50 ppm/K to -54 ppm/K for longitudinal extension. TCF should be roughly half of that value for extensional resonators since it is the dominant mechanism for frequency change. For the GaN resonators measured by the authors at the University of Michigan, the TCF values for length-extensional modes range from -14 ppm/K to -18 ppm/K [16], [17], [89], [90]. TCF values ranging from -23 ppm/K to -25 ppm/K are reported for thickness-extensional mode resonances of the devices reported in [16], [17], [89], and [90]. Larger TCF values of -27.6 ppm/K and -30 ppm/K are reported in [134] for thickness-extensional modes at resonance frequencies of 2.2 GHz and 8.7 GHz respectively. The larger measured TCF in [134] is most likely due to the thicker AlN and metal layers in the resonant stack with a larger TCE as compared to GaN. Also, specific material properties in different stacks (*e.g.*, different level of doping for unintentionally doped GaN) can cause variations in measured TCF values. Representative plots of the TCF for two fabricated length-extensional resonators are shown in (Fig. 28).

E. Power Handling and IIP₃

The ability to handle high power levels has always been one of the most attractive features of GaN-based electronics. This has spurred the growth of a large power-electronics industry. Electromechanical devices, especially resonators, also have limiting values of input power that can be handled without distortion of the output due to the onset of electrical and mechanical non-linearity. In piezoelectric resonators, mechanical non-linearity is primarily due to the non-linearity in the elastic coefficients of the material (especially for the suspension tethers) [62]. A popular method for characterizing the non-linearity and distortion of mechanical resonators associated with high input power levels is the third order intercept point (IIP₃). For GaN length-extensional mode resonators with thin tethers, distortion is seen at $+5$ dBm or greater, while no distortion is seen for clamped membrane type thickness-mode resonators at input powers up to $+20$ dBm [17]. Extrapolated IIP₃ (Fig. 29) demonstrate values in excess of $+32$ dBm without requiring the use of thick silicon structural

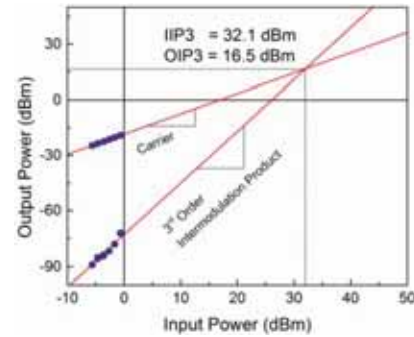


Fig. 29. Measured IIP₃ for a GaN mechanical resonator. The data are measured on a 2.1 GHz with a frequency separation of 50 kHz. The measured GaN bulk acoustic wave resonator shows Q of ~ 500 .

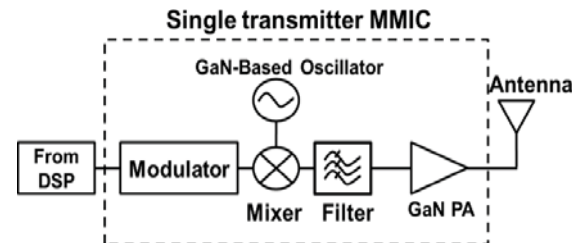


Fig. 30. A simplified schematic of a front-end transmitter based on all-GaN modules.

layers in the device, a method that is used in the AlN-on-Si TPOs configuration [62]. These values are comparable with similar devices made using AlN [135].

VI. FUTURE POSSIBILITIES

All-GaN integrated microsystems benefit from the combined advantages of piezoelectric properties of GaN for sensing and actuation and inherent gain in the AlGaIn/GaN HEMTs for signal amplification. In fact, integrated circuits with diverse functionalities can be realized based on electromechanical properties of GaN. GaN HEMTs and MEMS components, co-integrated with high- Q passives, such as capacitors and inductors can be used in timing and sensing applications. As an example of a critical application of integrated GaN microsystem, a simple transmitter MMIC schematic is shown in Fig. 30, where the preferred integration boundary of the power amplifier and other front-end components are demonstrated. GaN monolithic microwave integrated circuits (MMICs) provide better performance in terms of power, radiation hardness, and operation temperature, leading to products that could be used in harsh environments. Furthermore, future integration with GaN optoelectronic components is possible to incorporate diverse functionalities on the same GaN system.

GaN resonant systems can be used for a variety of physical, chemical, and biological sensing applications. Resonant IR detector arrays using GaN and GaN-on-Si structures have been demonstrated recently [57], [90], [92] (Fig. 31(a, b)) and have the potential to achieve highly sensitive IR detection with low susceptibility to background thermal noise. The same platform can be used for detecting small perturbations in temperature or mass. The wide bandgap of GaN also makes it a natural candidate for short wavelength optical detectors (Fig. 31(c, d)),

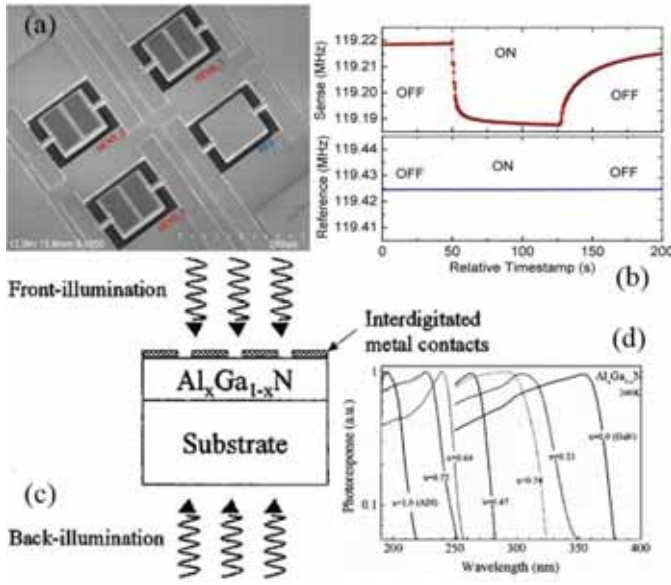


Fig. 31. (a) A 2×2 array of GaN-on-SOI length extensional resonators that is used as sensitive IR detector. The sensing scheme depends on the shift in mechanical resonance of the GaN resonator having an IR absorber coating. After [92]. The same platform can be used for other purposes by replacing the IR absorber by chemically or biologically selective absorber layers. (b) Measured response of a representative sense and reference resonant detector illuminated by near IR radiation. A differential scheme using a reference resonator corrects for ambient thermal fluctuations and other common mode signals. (c) A schematic and (d) measured photoresponse for photoconductive IR and solar blind UV detectors using $\text{Al}_x\text{Ga}_{1-x}\text{N}$ [136].

and the use of a compositionally tuned $\text{Al}_x\text{Ga}_{1-x}\text{N}$ alloy makes the spectral absorption selective [136]. Integration of a number of different spectrally selective sensors is possible on a single GaN substrate, which would enable multi-wavelength optical detection over a broad range.

A large number of mature GaN-based technologies such as RF electronics, power electronics, and LEDs along with emerging technologies such as GaN-based quantum dots, nanowires, and optical waveguides can be combined with GaN-based MEMS technology to address a variety of applications. Of special interest would be applications requiring operation of optical, mechanical, and electrical elements at high temperatures that conventional Si-based technologies cannot endure. Such GaN systems can be especially attractive for mining and harsh environment resource exploration, aerospace, and defense.

VII. CONCLUSION

In this paper, we reviewed the mechanical and electrical properties of GaN and AlGaN/GaN material systems grown on silicon substrate, with the aim to increase attention to this interesting material for use in NEMS/MEMS. In addition acoustic properties of GaN-based devices were investigated and compared to measured data, the result of which is valuable for the development of future high-power and low-loss GaN electronics. The discussed GaN microelectromechanical devices in conjunction with AlGaN/GaN HEMTs could enable low-noise, high-speed, and power devices and circuits for use in sensing, surveillance, electronic

warefare, multifunctional RF systems communications, and power applications.

REFERENCES

- [1] A. D. Hanser and K. R. Evans, "Development of the bulk GaN substrate market," in *Technology of Gallium Nitride Cryst. Growth*, vol. 133, D. Ehrentraut, E. Meissner, and M. Bockowski, Eds. Berlin, Germany: Springer-Verlag, 2010, pp. 3–27.
- [2] V. Cimalla, J. Pezoldt, and O. Ambacher, "Group III nitride and SiC based MEMS and NEMS: Materials properties, technology and applications," *J. Phys. D, Appl. Phys.*, vol. 40, no. 20, pp. 6386–6434, 2007.
- [3] S. Nakamura and M. R. Krames, "History of gallium-nitride-based light-emitting diodes for illumination," *Proc. IEEE*, vol. 101, no. 10, pp. 2211–2220, Oct. 2013.
- [4] R. Tabrizian, M. Rais-Zadeh, and F. Ayazi, "Effect of phonon interactions on limiting the f.Q product of micromechanical resonators," in *Proc. Int. Solid-State Sens., Actuators, Microsyst. Conf. (TRANSDUCERS)*, Denver, CO, USA, 2009, pp. 2131–2134.
- [5] S. Karmann, R. Helbig, and R. A. Stein, "Piezoelectric properties and elastic constants of 4H and 6H SiC at temperatures 4–320 K," *J. Appl. Phys.*, vol. 66, no. 8, pp. 3922–3924, 1989.
- [6] V. Siklitsky. (1998). *Semiconductors on NSM-Gallium Nitride*. [Online]. Available: <http://www.ioffe.ru/SVA/NSM/>, accessed Nov. 30, 2013.
- [7] M. Shur, S. Rumyantsev, and M. Levinstein, Eds., *SiC Materials and Devices*, vol. 1. Singapore: World Scientific, 2006.
- [8] S. Adachi, *Physical Properties of III-V Semiconductor Compounds*. Hoboken, NJ, USA: Wiley, 1992.
- [9] S. Adachi, *GaAs and Related Materials*. Singapore: World Scientific, 1994.
- [10] Q. Zou *et al.*, "High coupling coefficient temperature compensated FBAR resonator for oscillator application with wide pulling range," in *Proc. IEEE Int. Freq. Control Symp. (IFCS)*, Jun. 2010, pp. 646–651.
- [11] A. Konno *et al.*, "ScAlN Lamb wave resonator in GHz range released by XeF2 etching," in *Proc. IEEE Int. Ultrason. Symp. (IUS)*, Jul. 2013, pp. 1378–1381.
- [12] K. Umeda, H. Kawai, A. Honda, M. Akiyama, T. Kato, and T. Fukura, "Piezoelectric properties of ScAlN thin films for piezo-MEMS devices," in *Proc. IEEE 26th Int. Conf. Micro Electro Mech. Syst. (MEMS)*, Jan. 2013, pp. 733–736.
- [13] R. H. Olsson *et al.*, "Lamb wave micromechanical resonators formed in thin plates of lithium niobate," presented at the Solid-State Sens., Actuators, Microsyst. Workshop, Hilton Head, SC, USA, 2014, pp. 281–284.
- [14] H. Ledbetter, H. Ogi, and N. Nakamura, "Elastic, anelastic, piezoelectric coefficients of monocrystal lithium niobate," *Mech. Mater.*, vol. 36, no. 10, pp. 941–947, 2004.
- [15] V. J. Gokhale and M. Rais-Zadeh, "Phonon-electron interactions in piezoelectric semiconductor bulk acoustic wave resonators," *Sci. Rep.*, vol. 4, Jul. 2014, Art. ID 5617.
- [16] V. J. Gokhale, Y. Shim, and M. Rais-Zadeh, "Observation of the acoustoelectric effect in gallium nitride micromechanical bulk acoustic filters," in *Proc. IEEE Int. Freq. Control Symp. (IFCS)*, Jun. 2010, pp. 524–529.
- [17] V. J. Gokhale, J. Roberts, and M. Rais-Zadeh, "High performance bulk mode gallium nitride resonators and filters," in *Proc. 16th Int. Solid-State Sens., Actuators, Microsyst. Conf. (TRANSDUCERS)*, Beijing, China, 2011, pp. 926–929.
- [18] L. C. Popa and D. Weinstein, "L-band Lamb mode resonators in gallium nitride MMIC technology," in *Proc. IEEE Int. Freq. Control Symp. (IFCS)*, Taipei, Taiwan, May 2014, pp. 1–4.
- [19] S. Nakamura, M. Senoh, and T. Mukai, "Highly P-typed Mg-doped GaN films grown with GaN buffer layers," *Jpn. J. Appl. Phys.*, vol. 30, no. 10A, p. L1708, 1991.
- [20] A. Pinos *et al.*, "Excellent uniformity on large diameter GaN on silicon LED wafer," *Phys. Status Solidi C*, vol. 11, nos. 3–4, pp. 624–627, Apr. 2014.
- [21] Y. Golan *et al.*, "High-quality GaN on intentionally roughened c-sapphire," *Eur. Phys. J. Appl. Phys.*, vol. 22, no. 1, pp. 11–14, 2003.
- [22] M. Iwaya *et al.*, "Control of crystallinity of GaN grown on sapphire substrate by metalorganic vapor phase epitaxy using in situ X-ray diffraction monitoring method," *J. Cryst. Growth*, vol. 401, pp. 367–371, Sep. 2014.

- [23] S. Q. Zhou, A. Vantomme, B. S. Zhang, H. Yang, and M. F. Wu, "Comparison of the properties of GaN grown on complex Si-based structures," *Appl. Phys. Lett.*, vol. 86, no. 8, p. 081912, 2005.
- [24] A. Watanabe, T. Takeuchi, K. Hirose, H. Amano, K. Hiramatsu, and I. Akasaki, "The growth of single crystalline GaN on a Si substrate using AlN as an intermediate layer," *J. Cryst. Growth*, vol. 128, nos. 1–4, pp. 391–396, 1993.
- [25] N. Baron *et al.*, "The critical role of growth temperature on the structural and electrical properties of AlGaIn/GaN high electron mobility transistor heterostructures grown on Si(111)," *J. Appl. Phys.*, vol. 105, no. 3, pp. 033701-1–033701-8, 2009.
- [26] A. Soltani *et al.*, "Assessment of transistors based on GaN on silicon substrate in view of integration with silicon technology," *Semicond. Sci. Technol.*, vol. 28, no. 9, p. 094003, 2013.
- [27] H. P. D. Schenk, E. Frayssinet, A. Bavard, D. Rondi, Y. Cordier, and M. Kennard, "Growth of thick, continuous GaN layers on 4-in. Si substrates by metalorganic chemical vapor deposition," *J. Cryst. Growth*, vol. 314, no. 1, pp. 85–91, 2011.
- [28] A. Polian, M. Grimsditch, and I. Grzegory, "Elastic constants of gallium nitride," *J. Appl. Phys.*, vol. 79, no. 6, pp. 3343–3344, 1996.
- [29] J. Kolník, I. H. Oğuzman, K. F. Brennan, R. Wang, P. P. Ruden, and Y. Wang, "Electronic transport studies of bulk zincblende and wurtzite phases of GaN based on an ensemble Monte Carlo calculation including a full zone band structure," *J. Appl. Phys.*, vol. 78, no. 2, pp. 1033–1038, 1995.
- [30] A. F. Wright, "Elastic properties of zinc-blende and wurtzite AlN, GaN, and InN," *J. Appl. Phys.*, vol. 82, no. 6, pp. 2833–2839, 1997.
- [31] M. Yamaguchi *et al.*, "Brillouin scattering study of gallium nitride: Elastic stiffness constants," *J. Phys., Condens. Matter*, vol. 9, no. 1, p. 241, 1997.
- [32] M. D. Drory, J. W. Ager, III, T. Suski, I. Grzegory, and S. Porowski, "Hardness and fracture toughness of bulk single crystal gallium nitride," *Appl. Phys. Lett.*, vol. 69, no. 26, pp. 4044–4046, 1996.
- [33] R. Nowak *et al.*, "Elastic and plastic properties of GaN determined by nano-indentation of bulk crystal," *Appl. Phys. Lett.*, vol. 75, no. 14, pp. 2070–2072, 1999.
- [34] G. Yu *et al.*, "Mechanical properties of the GaN thin films deposited on sapphire substrate," *J. Cryst. Growth*, vols. 189–190, pp. 701–705, Jun. 1998.
- [35] S. O. Kucheyev *et al.*, "Nanoindentation of epitaxial GaN films," *Appl. Phys. Lett.*, vol. 77, no. 21, pp. 3373–3375, 2000.
- [36] C.-H. Tsai, S.-R. Jian, and J.-Y. Juang, "Berkovich nanoindentation and deformation mechanisms in GaN thin films," *Appl. Surf. Sci.*, vol. 254, no. 7, pp. 1997–2002, 2008.
- [37] M. Martyniuk, G. Parish, H. Marchand, P. T. Fini, S. P. DenBaars, and L. Faraone, "Nanoindentation of laterally overgrown epitaxial gallium nitride," *Electron. Mater. Lett.*, vol. 8, no. 2, pp. 111–115, 2012.
- [38] W. C. Oliver and G. M. Pharr, "An improved technique for determining hardness and elastic modulus using load and displacement sensing indentation experiments," *J. Mater. Res.*, vol. 7, no. 6, pp. 1564–1583, 1992.
- [39] A. D. Bykhovski, B. L. Gelmont, and M. S. Shur, "Elastic strain relaxation and piezoeffect in GaN-AlN, GaN-AlGaIn and GaN-InGaIn superlattices," *J. Appl. Phys.*, vol. 81, no. 9, pp. 6332–6338, 1997.
- [40] O. Ambacher *et al.*, "Electronics and sensors based on piezoelectric AlGaIn/GaN heterostructures," *Phys. Status Solidi C*, vol. 0, no. 6, pp. 1878–1907, Sep. 2003.
- [41] F. Bernardini, V. Fiorentini, and D. Vanderbilt, "Spontaneous polarization and piezoelectric constants of III–V nitrides," *Phys. Rev. B*, vol. 56, no. 16, pp. 10024–10027, 1997.
- [42] M. S. Shur, A. D. Bykhovski, and R. Gaska, "Piezoelectric and piezoelectric properties of GaN-based materials," in *Proc. MRS*, vol. 537, 1998.
- [43] C. Luo, D. R. Clarke, and J. R. Dryden, "The temperature dependence of the thermal conductivity of single crystal GaN films," *J. Electron. Mater.*, vol. 30, no. 3, pp. 138–146, 2001.
- [44] A. Jezowski *et al.*, "Thermal conductivity of GaN crystals in 4.2–300 K range," *Solid-State Commun.*, vol. 128, nos. 2–3, pp. 69–73, 2003.
- [45] W. Liu and A. A. Balandin, "Thermal conduction in Al_xGa_{1-x}N alloys and thin films," *J. Appl. Phys.*, vol. 97, no. 7, pp. 073710-1–073710-6, 2005.
- [46] J. Zou, D. Kotchetkov, A. A. Balandin, D. I. Florescu, and F. H. Pollak, "Thermal conductivity of GaN films: Effects of impurities and dislocations," *J. Appl. Phys.*, vol. 92, no. 5, pp. 2534–2539, 2002.
- [47] D. I. Florescu, V. M. Asnin, F. H. Pollak, R. J. Molnar, and C. E. C. Wood, "High spatial resolution thermal conductivity and Raman spectroscopy investigation of hydride vapor phase epitaxy grown n-GaN/sapphire (0001): Doping dependence," *J. Appl. Phys.*, vol. 88, no. 6, pp. 3295–3300, 2000.
- [48] M. D. Kamatagi, N. S. Sankeshwar, and B. G. Mulimani, "Thermal conductivity of GaN," *Diamond Rel. Mater.*, vol. 16, no. 1, pp. 98–106, 2007.
- [49] C. Deger *et al.*, "Sound velocity of Al_xGa_{1-x}N thin films obtained by surface acoustic-wave measurements," *Appl. Phys. Lett.*, vol. 72, no. 19, pp. 2400–2402, 1998.
- [50] V. Bougrov, "Gallium nitride (GaN)," in *Properties of Advanced Semiconductor Materials: GaN, AlN, InN, BN, SiC, SiGe*. Hoboken, NJ, USA: Wiley, 2001.
- [51] A. D. Bykhovski, V. V. Kaminski, M. S. Shur, Q. C. Chen, and M. A. Khan, "Pyroelectricity in gallium nitride thin films," *Appl. Phys. Lett.*, vol. 69, no. 21, pp. 3254–3256, 1996.
- [52] U. K. Mishra, P. Parikh, and W. Yi-Feng, "AlGaIn/GaN HEMTs—An overview of device operation and applications," *Proc. IEEE*, vol. 90, no. 6, pp. 1022–1031, Jun. 2002.
- [53] U. K. Mishra, L. Shen, T. E. Kazior, and Y.-F. Wu, "GaN-based RF power devices and amplifiers," *Proc. IEEE*, vol. 96, no. 2, pp. 287–305, Feb. 2008.
- [54] J. Kuzmik, A. Kostopoulos, G. Konstantinidis, J.-F. Carlin, A. Georgakilas, and D. Pogany, "InAlN/GaN HEMTs: A first insight into technological optimization," *IEEE Trans. Electron Devices*, vol. 53, no. 3, pp. 422–426, Mar. 2006.
- [55] A. Guedes, S. Shelton, R. Przybyla, I. Izyumin, B. Boser, and D. A. Horsley, "Aluminum nitride pMUT based on a flexurally-suspended membrane," in *Proc. 16th Int. Solid-State Sens., Actuators, Microsyst. Conf. (TRANSDUCERS)*, Jun. 2011, pp. 2062–2065.
- [56] P. Muralt and J. Baborowski, "Micromachined ultrasonic transducers and acoustic sensors based on piezoelectric thin films," *J. Electrochem.*, vol. 12, nos. 1–2, pp. 101–108, 2004.
- [57] V. J. Gokhale, Y. Sui, and M. Rais-Zadeh, "Novel uncooled detector based on gallium nitride micromechanical resonators," *Proc. SPIE*, vol. 8353, pp. 835319-1–835319-6, May 2012.
- [58] L. C. Popa and D. Weinstein, "2DEG electrodes for piezoelectric transduction of AlGaIn/GaN MEMS resonators," in *Proc. Joint Eur. Freq. Time Forum Int. Freq. Control Symp. (EFTF/IFCS)*, Jul. 2013, pp. 922–925.
- [59] L. C. Popa and D. Weinstein, "Switchable piezoelectric transduction in AlGaIn/GaN MEMS resonators," in *Proc. Int. Solid-State Sens., Actuators, Microsyst. (TRANSDUCERS EUROSENSORS)*, Jun. 2013, pp. 2461–2464.
- [60] A. Ansari, V. J. Gokhale, J. Roberts, and M. Rais-Zadeh, "Monolithic integration of GaN-based micromechanical resonators and HEMTs for timing applications," in *Proc. IEEE Int. Electron Devices Meeting (IEDM)*, Dec. 2012, pp. 15.5.1–15.5.4.
- [61] A. Ansari and M. Rais-Zadeh, "HEMT-based read-out of a thickness-mode AlGaIn/GaN resonator," in *Proc. IEEE Int. Electron Devices Meeting (IEDM)*, Dec. 2013, pp. 18.3.1–18.3.4.
- [62] R. Abdolvand and F. Ayazi, "Enhanced power handling and quality factor in thin-film piezoelectric-on-substrate resonators," in *Proc. IEEE Ultrason. Symp.*, Oct. 2007, pp. 608–611.
- [63] G. K. Ho, R. Abdolvand, A. Sivapurapu, S. Humad, and F. Ayazi, "Piezoelectric-on-silicon lateral bulk acoustic wave micromechanical resonators," *J. Microelectromech. Syst.*, vol. 17, no. 2, pp. 512–520, Apr. 2008.
- [64] R. Abdolvand and F. Ayazi, "High-frequency monolithic thin-film piezoelectric-on-substrate filters," *Int. J. Microw. Wireless Technol.*, vol. 1, no. 1, pp. 29–35, 2009.
- [65] R. Abdolvand, H. M. Lavasani, G. K. Ho, and F. Ayazi, "Thin-film piezoelectric-on-silicon resonators for high-frequency reference oscillator applications," *IEEE Trans. Ultrason., Ferroelectr., Freq. Control*, vol. 55, no. 12, pp. 2596–2606, Dec. 2008.
- [66] P. Perlin, C. Jauberthie-Carillon, J. P. Itie, A. S. Miguel, I. Grzegory, and A. Polian, "Raman scattering and X-ray-absorption spectroscopy in gallium nitride under high pressure," *Phys. Rev. B*, vol. 45, no. 1, pp. 83–89, 1992.
- [67] E. A. Henriksen *et al.*, "Acoustic phonon scattering in a low density, high mobility AlGaIn/GaN field-effect transistor," *Appl. Phys. Lett.*, vol. 86, no. 25, pp. 252108-1–252108-3, 2005.
- [68] V. W. L. Chin, T. L. Tansley, and T. Osotchan, "Electron mobilities in gallium, indium, and aluminum nitrides," *J. Appl. Phys.*, vol. 75, no. 11, pp. 7365–7372, 1994.

- [69] D. Pavlidis, "GaN negative differential resistance components with terahertz operation capability: From fundamentals to devices," in *Optoelectronic Devices: III Nitrides*, M. Razeghi and M. Henini, Eds. New York, NY, USA: Elsevier, 2005, pp. 351–386.
- [70] Y. V. Gulyaev and F. S. Hickernell, "Acoustoelectronics: History, present state, and new ideas for a new era," *Acoust. Phys.*, vol. 51, no. 1, pp. 81–88, 2005.
- [71] H. J. Mckim, A. R. Hutson, and T. B. Bateman, "Some measurements of wave velocities and elastic moduli for cadmium sulphide," *J. Acoust. Soc. Amer.*, vol. 33, no. 6, pp. 856–862, 1961.
- [72] A. R. Hutson and D. L. White, "Elastic wave propagation in piezoelectric semiconductors," *J. Appl. Phys.*, vol. 33, no. 1, pp. 40–47, 1962.
- [73] M. Pomerantz, "Ultrasonic loss and gain mechanisms in semiconductors," *Proc. IEEE*, vol. 53, no. 10, pp. 1438–1451, Oct. 1965.
- [74] S. Strite and H. Morkoç, "GaN, AlN, and InN: A review," *J. Vac. Sci. Technol. B*, vol. 10, no. 4, pp. 1237–1266, 1992.
- [75] S. Yoshida, S. Misawa, and S. Gonda, "Epitaxial growth of GaN/AlN heterostructures," *J. Vac. Sci. Technol. B*, vol. 1, no. 2, pp. 250–253, 1983.
- [76] H. Amano, N. Sawaki, I. Akasaki, and Y. Toyoda, "Metalorganic vapor phase epitaxial growth of a high quality GaN film using an AlN buffer layer," *Appl. Phys. Lett.*, vol. 48, no. 5, pp. 353–355, 1986.
- [77] A. Duwel, R. N. Candler, T. W. Kenny, and M. Varghese, "Engineering MEMS resonators with low thermoelastic damping," *J. Microelectromech. Syst.*, vol. 15, no. 6, pp. 1437–1445, 2006.
- [78] V. A. Thakar, Z. Wu, A. Peczkalski, and M. Rais-Zadeh, "Piezoelectrically transduced temperature-compensated flexural-mode silicon resonators," *J. Microelectromech. Syst.*, vol. 22, no. 3, pp. 815–823, Jun. 2013.
- [79] S. B. Lisesivdin, A. Yildiz, N. Balkan, M. Kasap, S. Ozcelik, and E. Ozbay, "Scattering analysis of two-dimensional electrons in AlGaIn/GaN with bulk related parameters extracted by simple parallel conduction extraction method," *J. Appl. Phys.*, vol. 108, no. 1, p. 013712, 2010.
- [80] T. Palacios *et al.*, "Wet etching of GaN grown by molecular beam epitaxy on Si(111)," *Semicond. Sci. Technol.*, vol. 15, no. 10, pp. 996–1000, 2000.
- [81] D. Huang *et al.*, "Dependence of GaN polarity on the parameters of the buffer layer grown by molecular beam epitaxy," *Appl. Phys. Lett.*, vol. 78, no. 26, pp. 4145–4147, 2001.
- [82] P. Visconti, K. M. Jones, M. A. Reshchikov, R. Cingolani, H. Morkoç, and R. J. Molnar, "Dislocation density in GaN determined by photoelectrochemical and hot-wet etching," *Appl. Phys. Lett.*, vol. 77, no. 22, pp. 3532–3534, 2000.
- [83] D. Zhuang and J. H. Edgar, "Wet etching of GaN, AlN, and SiC: A review," *Mater. Sci. Eng., R, Rep.*, vol. 48, no. 1, pp. 1–46, 2005.
- [84] M. S. Minsky, M. White, and E. L. Hu, "Room-temperature photoenhanced wet etching of GaN," *Appl. Phys. Lett.*, vol. 68, no. 11, pp. 1531–1533, 1996.
- [85] A. R. Stonas, N. C. MacDonald, K. L. Turner, S. P. DenBaars, and E. L. Hu, "Photoelectrochemical undercut etching for fabrication of GaN microelectromechanical systems," *J. Vac. Sci. Technol. B*, vol. 19, no. 6, pp. 2838–2841, 2001.
- [86] R. Prashanth, K. Sriram, R. Siddharth, and N. W. Gregory, "Fabrication and characterization of a piezoelectric gallium nitride switch for optical MEMS applications," *Smart Mater. Struct.*, vol. 21, no. 9, p. 094003, 2012.
- [87] D. A. Stocker, E. F. Schubert, and J. M. Redwing, "Crystallographic wet chemical etching of GaN," *Appl. Phys. Lett.*, vol. 73, no. 18, pp. 2654–2656, 1998.
- [88] S. J. Pearton, R. J. Shul, G. F. McLane, and C. Constantine, "Reactive ion etching of III–V nitrides," *Solid-State Electron.*, vol. 41, no. 2, pp. 159–163, 1997.
- [89] A. Ansari, V. J. Gokhale, V. A. Thakar, J. Roberts, and M. Rais-Zadeh, "Gallium nitride-on-silicon micromechanical overtone resonators and filters," in *Proc. IEEE Int. Electron Devices Meeting (IEDM)*, Dec. 2011, pp. 20.3.1–20.3.4.
- [90] V. J. Gokhale and M. Rais-Zadeh, "Sensitive uncooled IR detectors using gallium nitride resonators and silicon nitride absorbers," in *Proc. Solid-State Sens., Actuators, Microsyst. Workshop*, Hilton Head Island, SC, USA, 2012, pp. 46–49.
- [91] A. Ansari and M. Rais-Zadeh, "A thickness-mode AlGaIn/GaN resonant body high electron mobility transistor," *IEEE Trans. Electron Devices*, vol. 61, no. 4, pp. 1006–1013, Apr. 2014.
- [92] V. J. Gokhale and M. Rais-Zadeh, "Uncooled infrared detectors using gallium nitride on silicon micromechanical resonators," *J. Microelectromech. Syst.*, vol. 23, no. 4, pp. 803–810, 2013.
- [93] S. Gautier *et al.*, "Structural and compositional characterization of MOVPE GaN thin films transferred from sapphire to glass substrates using chemical lift-off and room temperature direct wafer bonding and GaN wafer scale MOVPE growth on ZnO-buffered sapphire," *J. Cryst. Growth*, vol. 370, pp. 63–67, May 2013.
- [94] W. S. Wong, T. Sands, and N. W. Cheung, "Damage-free separation of GaN thin films from sapphire substrates," *Appl. Phys. Lett.*, vol. 72, no. 5, pp. 599–601, 1998.
- [95] C. Jaeyi *et al.*, "Transfer of GaN LEDs from sapphire to flexible substrates by laser lift-off and contact printing," *IEEE Photon. Technol. Lett.*, vol. 24, no. 23, pp. 2115–2118, Dec. 1, 2012.
- [96] A. Tazuin *et al.*, "Transfers of 2-inch GaN films onto sapphire substrates using Smart Cut™ technology," *Electron. Lett.*, vol. 41, no. 11, pp. 668–670, 2005. [Online]. Available: http://digital-library.theiet.org/content/journals/10.1049/el_20051038
- [97] K. K. Ryu, J. C. Roberts, E. L. Piner, and T. Palacios, "Thin-body N-face GaN transistor fabricated by direct wafer bonding," *IEEE Electron Device Lett.*, vol. 32, no. 7, pp. 895–897, Jul. 2011.
- [98] Soitech. (2013). Available: <http://www.soitech.com/en/>
- [99] K. Brueckner *et al.*, "Resonant piezoelectric AlGaIn/GaN MEMS sensors in longitudinal mode operation," in *Proc. IEEE Int. Conf. Micro Electro Mech. Syst. (MEMS)*, Jan. 2009, pp. 927–930.
- [100] F. Niebelschuetz *et al.*, "Piezoelectric actuated epitaxially grown AlGaIn/GaN-resonators," *Phys. Status Solidi C*, vol. 7, nos. 7–8, pp. 1829–1831, 2010.
- [101] A. Ansari and M. Rais-Zadeh, "An 8.7 GHz GaN micromechanical resonator with an integrated AlGaIn/GaN HEMT," in *Proc. Solid-State Sens., Actuators, Microsyst. Workshop*, Hilton Head Island, SC, USA, 2014.
- [102] V. Tilak, A. Vertiatchikh, J. Jiang, N. Reeves, and S. Dasgupta, "Piezoresistive and piezoelectric effects in GaN," *Phys. Status Solidi C*, vol. 3, no. 6, pp. 2307–2311, 2006.
- [103] A. Talukdar, M. Qazi, and G. Koley, "High frequency dynamic bending response of piezoresistive GaN microcantilevers," *Appl. Phys. Lett.*, vol. 101, no. 25, p. 252102, 2012.
- [104] A. Talukdar, M. Qazi, and G. Koley, "Static and dynamic responses of GaN piezoresistive microcantilever with embedded AlGaIn/GaN HFET for sensing applications," in *Proc. IEEE Sensors*, Nov. 2013, pp. 1–4.
- [105] M. Chu *et al.*, "Strain effects in AlGaIn/GaN HEMTs," in *Materials and Reliability Handbook for Semiconductor Optical and Electron Devices*, U. Osamu and S. J. Pearton, Eds. New York, NY, USA: Springer, 2013.
- [106] M. Chu, A. D. Koehler, A. Gupta, T. Nishida, and S. E. Thompson, "Simulation of AlGaIn/GaN high-electron-mobility transistor gauge factor based on two-dimensional electron gas density and electron mobility," *J. Appl. Phys.*, vol. 108, no. 10, pp. 104502-1–104502-6, 2010.
- [107] J. M. Gray, C. T. Rogers, K. A. Bertness, and N. A. Sanford, "Gallium nitride nanowire electromechanical resonators with piezoresistive read-out," *J. Vac. Sci. Technol. B, Microelectron. Nanometer Struct.*, vol. 29, no. 5, pp. 052001-1–052001-4, 2011.
- [108] F. Niebelschütz *et al.*, "AlGaIn/GaN-based MEMS with two-dimensional electron gas for novel sensor applications," *Phys. Status Solidi C*, vol. 5, no. 6, pp. 1914–1916, 2008.
- [109] F. Niebelschütz *et al.*, "Resonant MEMS based on cubic GaN layers," *Phys. Status Solidi C*, vol. 7, no. 1, pp. 116–119, 2010.
- [110] K. Brueckner *et al.*, "Micro- and nano-electromechanical resonators based on SiC and group III-nitrides for sensor applications," *Phys. Status Solidi A*, vol. 208, no. 2, pp. 357–376, 2011.
- [111] A. Ben Amar *et al.*, "Bias dependence of gallium nitride micro-electromechanical systems actuation using a two-dimensional electron gas," *Appl. Phys. Exp.*, vol. 5, no. 6, p. 067201, 2012.
- [112] L.-W. Hung and C. T.-C. Nguyen, "Capacitive-piezoelectric AlN resonators with $Q > 12,000$," in *Proc. IEEE 24th Int. Conf. Micro Electro Mech. Syst. (MEMS)*, Jan. 2011, pp. 173–176.
- [113] C. Cassella, J. Segovia-Fernandez, and G. Piazza, "Segmented electrode excitation of aluminum nitride contour mode resonators to optimize the device figure of merit," in *Proc. 17th Int. Solid-State Sens., Actuators, Microsyst. (TRANSDUCERS EUROSENSORS)*, 2013, pp. 506–509.
- [114] Y.-R. Wu and J. Singh, "Polar heterostructure for multifunction devices: Theoretical studies," *IEEE Trans. Electron Devices*, vol. 52, no. 2, pp. 284–293, Feb. 2005.

- [115] M. Faucher *et al.*, "Amplified piezoelectric transduction of nanoscale motion in gallium nitride electromechanical resonators," *Appl. Phys. Lett.*, vol. 94, no. 23, pp. 233506-1–233506-3, 2009.
- [116] S.-H. Lee, H.-H. Jeong, S.-B. Bae, H.-C. Choi, J.-H. Lee, and Y.-H. Lee, "Epitaxially grown GaN thin-film SAW filter with high velocity and low insertion loss," *IEEE Trans. Electron Devices*, vol. 48, no. 3, pp. 524–529, Mar. 2001.
- [117] T. Palacios *et al.*, "High frequency SAW devices on AlGaIn: Fabrication, characterization and integration with optoelectronics," in *Proc. IEEE Ultrason. Symp.*, Oct. 2002, pp. 57–60.
- [118] A. Müller *et al.*, "SAW devices manufactured on GaN/Si for frequencies beyond 5 GHz," *IEEE Electron Device Lett.*, vol. 31, no. 12, pp. 1398–1400, Dec. 2010.
- [119] K.-Y. Wong, W. Tang, K. M. Lau, and K. J. Chen, "Planar two-dimensional electron gas (2DEG) IDT SAW filter on AlGaIn/GaN heterostructure," in *Proc. IEEE/MTT-S Int. Microw. Symp. (IMS)*, Jun. 2007, pp. 2043–2046.
- [120] L. Shao, M. Zhang, A. Banerjee, P. Bhattacharya, and K. P. Pipe, "Emission and detection of surface acoustic waves by AlGaIn/GaN high electron mobility transistors," *Appl. Phys. Lett.*, vol. 99, no. 24, p. 243507, 2011.
- [121] M. Faucher, G. Martin, J.-M. Friedt, and S. Ballandras, "A 1 GHz SAW oscillator on epitaxial GaN/Si substrate: Toward co-integrated frequency sources," in *Proc. Joint Eur. Freq. Time Forum Int. Freq. Control Symp. (EFTF/IFCS)*, Jul. 2013, pp. 21–24.
- [122] V. B. Braginsky and V. P. Mitrofanov, *Systems With Small Dissipation*, K. S. Thorne, Ed. Chicago, IL, USA: Univ. Chicago Press, pp. 1–42, 1985.
- [123] V. T. Srikanth and S. D. Senturia, "Thermoelastic damping in fine-grained polysilicon flexural beam resonators," *J. Microelectromech. Syst.*, vol. 11, no. 5, pp. 499–504, Oct. 2002.
- [124] S. A. Chandorkar, M. Agarwal, R. Melamud, R. N. Candler, K. E. Goodson, and T. W. Kenny, "Limits of quality factor in bulk-mode micromechanical resonators," in *Proc. IEEE 21st Int. Conf. Micro Electro Mech. Syst. (MEMS)*, Jan. 2008, pp. 74–77.
- [125] A. Müller *et al.*, "6.3-GHz film bulk acoustic resonator structures based on a gallium nitride/silicon thin membrane," *IEEE Electron Device Lett.*, vol. 30, no. 8, pp. 799–801, Aug. 2009.
- [126] J. Kaitila, "BAW device basics," in *RF Bulk Acoustic Wave Filters for Communications*, K.-Y. Hashimoto, Ed. Norwood, MA, USA: Artech House, 2009, pp. 51–90.
- [127] R. Wang, S. A. Bhavne, and K. Bhattacharjee, "High $k_t^2 \times Q$, multi-frequency lithium niobate resonators," in *Proc. IEEE Int. Conf. Micro Electro Mech. Syst. (MEMS)*, Jan. 2013, pp. 165–168.
- [128] R. Ruby, P. Bradley, J. Larson, III, Y. Oshmyansky, and D. Figueredo, "Ultra-miniature high-Q filters and duplexers using FBAR technology," in *Proc. IEEE Int. Solid-State Circuits Conf. (ISSCC)*, Feb. 2001, pp. 120–121.
- [129] C. Durand *et al.*, "In-plane silicon-on-nothing nanometer-scale resonant suspended gate MOSFET for in-IC integration perspectives," *IEEE Electron Device Lett.*, vol. 29, no. 5, pp. 494–496, May 2008.
- [130] D. Grogg, M. Mazza, D. Tsamados, and A. M. Ionescu, "Multi-gate vibrating-body field effect transistor (VB-FETs)," in *Proc. IEEE Int. Electron Devices Meeting (IEDM)*, Dec. 2008, pp. 1–4.
- [131] D. Weinstein and S. A. Bhavne, "The resonant body transistor," *Nano Lett.*, vol. 10, no. 4, pp. 1234–1237, 2010.
- [132] M. Faucher, Y. Cordier, M. Werquin, L. Buchailot, C. Gaquiere, and D. Theron, "Electromechanical transconductance properties of a GaN MEMS resonator with fully integrated HEMT transducers," *J. Microelectromech. Syst.*, vol. 21, no. 2, pp. 370–378, Apr. 2012.
- [133] R. Ram Yadav and D. K. Pandey, "Ultrasonic characterisation of gallium nitride," *Mater. Res. Innov.*, vol. 10, no. 4, pp. 402–407, 2006.
- [134] A. Ansari and M. Rais-Zadeh, "A temperature-compensated micro-mechanical gallium nitride resonator," *IEEE Electron Device Lett.*, to be published.
- [135] C. D. Nordquist and R. H. Olsson, "Power handling and intermodulation distortion of contour-mode AlN MEMS resonators and filters," in *Proc. IEEE/MTT-S Int. Microw. Symp. (IMS)*, Jun. 2011, pp. 1–4.
- [136] M. Razeghi, "Short-wavelength solar-blind detectors-status, prospects, and markets," *Proc. IEEE*, vol. 90, no. 6, pp. 1006–1014, Jun. 2002.



Mina Rais-Zadeh (S'03–M'08–SM'12) received the B.S. degree in electrical engineering from the Sharif University of Technology, Tehran, Iran, in 2002, and the M.S. and Ph.D. degrees in electrical and computer engineering from the Georgia Institute of Technology, Atlanta, GA, USA, in 2005 and 2008, respectively. From 2008 to 2009, she was a Post-Doctoral Research Fellow with the Georgia Institute of Technology. Since 2009, she has been with the University of Michigan, Ann Arbor, MI, USA, where she is currently an Associate Professor of Electrical

Engineering and Computer Science.

She was a recipient of the NSF CAREER Award (2011), the IEEE Electron Device Society's Early Career Award (2011), the NASA Early Career Faculty Award (2012), the Crosby Research Award from the University of Michigan (2013), and the ONR Young Investigator Award (2014). She was one of the 81 invitees by the National Academy of Engineering to attend the 19th Annual Frontiers of Engineering Symposium (2013). Together with her students, she received several best paper awards at the Transducers Conference, the IEEE SIRC conferences, and the International Microwave Symposia. She is a member of the 2014 IEDM Executive Committee and the 2015 IEEE MEMS Executive Committee, and has served as a Technical Program Committee Member of the IEEE International Electron Devices Meeting (2011–2013), the IEEE Sensors Conference (2011–2014), the Hilton Head Workshop (2012, 2014), the IEEE MEMS Conference (2014–2015), the Transducers Conference (2015), and the International Frequency Control Symposium (2015). She is an Associate Editor of the IEEE ELECTRON DEVICE LETTERS. Her research interests include electron devices for wireless communication and sensing applications and the related device physics, resonant micromechanical devices, RF microelectromechanical systems (MEMS), gallium nitride MEMS, and micro/nano fabrication process development.



Vikrant Jayant Gokhale (S'10) received the B.Tech. degree in electronics and instrumentation engineering from the Vellore Institute of Technology, Vellore, India, in 2007, and the M.S. and Ph.D. degrees in electrical and computer engineering from the University of Michigan, Ann Arbor, MI, USA, in 2010 and 2014, respectively.

He was an Engineer with Honeywell Technology Solutions, Sensing, and Control, Bangalore, India, from 2007 to 2008. Since 2014, he has been a Post-Doctoral Researcher with the Physical Measurement Laboratory, National Institute of Standards and Technology, Gaithersburg, MD, USA. His specific research interests include high-frequency microelectromechanical systems (MEMS) resonators and associated energy loss mechanisms, and resonant MEMS sensors for detecting physical phenomena, such as infrared radiation.



Azadeh Ansari (S'10) received the B.S. degree in electrical engineering from the Sharif University of Technology, Tehran, Iran, in 2010. She joined the University of Michigan, Ann Arbor, MI, USA, in 2011, where she received the M.S. degree in 2013 and is currently pursuing the Ph.D. degree. Her research interests include GaN-based micromechanical resonators, integration of GaN HEMTs and microelectromechanical systems (MEMS), resonant transistors, and interface circuit design for MEMS.



Marc Faucher received the M.S. degree in physics from the University of Marseille, Marseille, France, in 2002; the Engineer's degree from École Centrale de Marseille, Marseille; and the Ph.D. degree in physics from Joseph Fourier University, Grenoble, France, in 2003, where he studied superconducting nanocircuits.

He was a Post-Doctoral Researcher with the Atomic Energy Commission-Laboratory for Electronics and Information Technology, Grenoble, from 2003 to 2005, where he was worked on semiconductor characterization techniques. He joined the Institute of Electronics, Microelectronics, and Nanotechnology (IEMN), Lille, France (CNRS UMR 8520), in 2006, as a Post-Doctoral Researcher.

Dr. Faucher is currently a Centre National de la Recherche Scientifique Researcher with the Nano and Microsystems Group, IEMN. His research is related to microelectromechanical systems (MEMS) and nanoelectromechanical systems, including silicon resonators for high-frequency sensing systems, micro/nanofabrication, and the design, fabrication, and characterization of gallium nitride MEMS/high-electron mobility transistors.



Didier Théron was born in Auxerre, France, in 1962. He received the Dipl.-Ing. degree from École Polytechnique, Palaiseau, France, in 1984; the Master's degree in solid-state physics from the University of Paris-Sud, Orsay, France, in 1985; and the Ph.D. degree in physics from the Swiss Federal Institute of Technology, Lausanne, Switzerland, in 1989, with a focus on the physical simulation and MBE growth of GaAs-based multichannel HEMTs. Since 1990, he has been with the Centre National de la Recherche Scientifique (CNRS), Paris, where

he is currently the Research Director. He is performing his research activity with the Institute of Electronics, Microelectronics, and Nanotechnology, Villeneuve d'Ascq, France, where he worked on the physics and technology of GaAs and InP-based power HEMTs for millimeter-wave applications (from 10 to 94 GHz). He worked on GaN HEMTs in cooperation with the Alcatel/Thales III-V Laboratory, Palaiseau. Since 2006, he has worked on GaN microelectromechanical systems (MEMS) resonator physics. He is also involved in Si MEMS resonator device physics for atomic force detection and RF electrical property characterization of dielectric materials using scanning microwave microscopy developed in cooperation with Agilent Technologies, Santa Clara, CA, USA.

He has been successively involved in research administration as a Scientific Advisor of Microelectronics with CNRS, the Program Director of Nanotechnology and Nanosystems with the National Research Agency, and more recently, an Advisor of Nanotechnology with the French Ministry of Research, since 2004. He has authored about 120 publications and communications, and was a recipient of the Bronze Medal from CNRS in 1998.



Yvon Cordier was born in France in 1965. He received the degree in materials science engineering from the EUDIL School of Engineering, University of Lille, Villeneuve-d'Ascq, France, in 1988, and the Ph.D. degree from the Lille University of Science and Technology, Villeneuve-d'Ascq, in 1992. In 1991, he joined the Central Research Laboratory of Thomson-CSF, Orsay, France, where he developed III-V epitaxial structures for electronic and optoelectronic devices. In 1996, he joined the Institute of Electronics, Microelectronics, and Nanotechnology, Villeneuve d'Ascq, France, as a Centre National de la Recherche Scientifique (CNRS) permanent Researcher, and studied the growth of AlInAs/GaInAs metamorphic heterostructures on GaAs substrate. In 2001, he joined the Centre de Recherche sur l'HétéroÉpitaxie et ses Applications-CNRS, Valbonne, France. He has authored or co-authored over 180 publications, holds two patents, and is heading, as the Research Director, a team working on the growth of semiconductor materials, including GaN, SiC, Graphene, and ZnO, for electronics.



Lionel Buchaillet is currently a Centre National de la Recherche Scientifique (CNRS) Senior Researcher. He received the M.S. degree in material sciences and the Ph.D. degree in mechanical engineering from the Université de Franche-Comté, Besançon, France, in 1991 and 1995, respectively. From 1995 to 1997, he was with the Laboratory for Integrated MicroMechatronic Systems-CNRS-IIS, University of Tokyo, Tokyo, Japan, as a JSPS Post-Doctoral Fellow working on thin-film shape memory alloys actuators for microelectromechanical systems (MEMS). In 1997, he was a Research and Development Engineer with SAFRAN, Paris, France, and AVIAC Technologies, Mantes-la-Jolie, France. In 1998, he joined the Department of ISEN, CNRS, Institute of Electronics, Microelectronics and Nanotechnology (IEMN), Villeneuve d'Ascq, France. He was the Head of the Silicon-Based MEMS Research Group at IEMN from 2001 to 2009. In 2010, he became the Director of IEMN. His research focuses on mechanical sensors and systems, RF MEMS/MEMS for microwaves, and scientific micro and nanoinstruments. He has authored or co-authored over 100 papers and several book chapters. He is an Editor of the IEEE JOURNAL OF MICROELECTROMECHANICAL SYSTEMS and the IOP's *Journal of Micromechanics and Microengineering*. He was a recipient of the CNRS Bronze Medal.